nature aging

LETTERS

https://doi.org/10.1038/s43587-021-00158-9

Check for updates

Dissection of the polygenic architecture of neuronal Aβ production using a large sample of individual iPSC lines derived from Alzheimer's disease patients

Takayuki Kondo[1,2,3], Norikazu Hara[4], Satoshi Koyama[5], Yuichiro Yada[2,3], Kayoko Tsukita[2,3], Ayako Nagahashi[1,2], Takeshi Ikeuchi[4], Kenji Ishii[6], Takashi Asada[7], Tetsuaki Arai[7], Ryo Yamada[5], Alzheimer's Disease Neuroimaging Initiative (ADNI)*, Japanese Alzheimer's Disease Neuroimaging Initiative (J-ADNI)* and Haruhisa Inoue[1,2,3,8] ✉

Genome-wide association studies have demonstrated that polygenic risks shape Alzheimer's disease (AD). To elucidate the polygenic architecture of AD phenotypes at a cellular level, we established induced pluripotent stem cells from 102 patients with AD, differentiated them into cortical neurons and conducted a genome-wide analysis of the neuronal production of amyloid β (Aβ). Using such a cellular dissection of polygenicity (CDiP) approach, we identified 24 significant genome-wide loci associated with alterations in Aβ production, including some loci not previously associated with AD, and confirmed the influence of some of the corresponding genes on Aβ levels by the use of small interfering RNA. CDiP genotype sets improved the predictions of amyloid positivity in the brains and cerebrospinal fluid of patients in the Alzheimer's Disease Neuroimaging Initiative (ADNI) cohort. Secondary analyses of exome sequencing data from the Japanese ADNI and the ADNI cohorts focused on the 24 CDiP-derived loci associated with alterations in Aβ led to the identification of rare AD variants in KCNMA1.

An abundance of genetic research on Alzheimer's disease (AD) has provided plentiful evidence that late-onset AD has heritability estimates of 56–79%[1]. After the advance of genomic cohort research and establishment of the human genome database, genome-wide association study (GWAS) has enabled us to investigate the genetic backgrounds associated with diverse human traits[2] and specified more than 50 loci as AD-associated genes[3]. Although previous GWASs of onset age, brain atrophy or biomarkers in serum or cerebrospinal fluid (CSF)[4–9] have revealed the genetic background, cellular polygenicity behind the disease pathomechanism has as yet not been clearly elucidated[10,11,16]. In this study, we conducted genome-wide analysis by using amyloid β (Aβ), produced from induced pluripotent stem cell (iPSC)-derived cortical neurons in an AD cohort, as a pathological trait. We then conducted cellular dissection of polygenicity (CDiP) to reveal a complex pathomechanism in a neuron-specific manner (Fig. 1a).

To analyze the AD pathology of neurons, we established iPSCs from patients in a sporadic AD (SAD) cohort ($N=102$) (Fig. 1b,c and Extended Data Fig. 1a,b) and established iPSCs showing normal karyotype and in vitro ability to generate all three embryonic germ layers as well as X-inactive specific transcript (*XIST*) similar to that of human embryonic stem cells[12] (Supplementary Table 1). We directly differentiated all iPSC clones into cortical neurons by forced expression of the human *NGN2* gene (Extended Data Fig. 1c–f)[13]. In this differentiation protocol, exogenous *NGN2* was well suppressed after day 8 and Aβ phenotypes were constant from days 8 to 14. The complex AD pathology consists of various kinds of molecules or biological events like Aβ and tau, which can be candidates of GWAS traits. We selected Aβ for a pathological trait in cortical neurons because Aβ is a triggering molecule in the initiation of a long-term pathological cascade of AD, resulting in dementia[14,15]. We quantified Aβ40 and Aβ42, as protective and toxic Aβ, respectively and the Aβ42/40 ratio in the culture supernatant of SAD cortical neurons. The *APP* and *PSEN1* genes, which play a central role in the Aβ production pathway, are known to affect neural development[16–19] and neural differentiation propensity from human iPSCs[20]. Therefore, when evaluating Aβ among different patients' iPSCs, it is important to maintain homogenous purity of neuronal differentiation and to normalize variability in the number of neurons per well. The direct differentiation method used in this study results in uniform and high-purity cortical neurons (Extended Data Fig. 1d–f), but evokes variability in neuronal density among patients due to the stress of direct conversion from day 0 to day 5 (Extended Data Fig. 1c,d) and this variability will affect the amount of Aβ. To normalize the variability in the number of neurons per well, we used the total protein concentration extracted from the neurons in the whole well, as changes in protein concentration linearly reflected

[1]Medical-risk Avoidance based on iPS Cells Team, RIKEN Center for Advanced Intelligence Project (AIP), Kyoto, Japan. [2]Center for iPS Cell Research and Application (CiRA), Kyoto University, Kyoto, Japan. [3]iPSC-based Drug Discovery and Development Team, RIKEN BioResource Research Center (BRC), Kyoto, Japan. [4]Department of Molecular Genetics, Brain Research Institute, Niigata University, Niigata, Japan. [5]Unit of Statistical Genetics, Center for Genomic Medicine, Graduate School of Medicine, Kyoto University, Kyoto, Japan. [6]Research Team for Neuroimaging, Tokyo Metropolitan Institute of Gerontology, Tokyo, Japan. [7]Department of Psychiatry, Division of Clinical Medicine, Faculty of Medicine, University of Tsukuba, Ibaraki, Japan. [8]Institute for Advancement of Clinical and Translational Science (iACT), Kyoto University Hospital, Kyoto, Japan. *A list of participants and their affiliations appear at the end of the paper. ✉e-mail: haruhisa@cira.kyoto-u.ac.jp

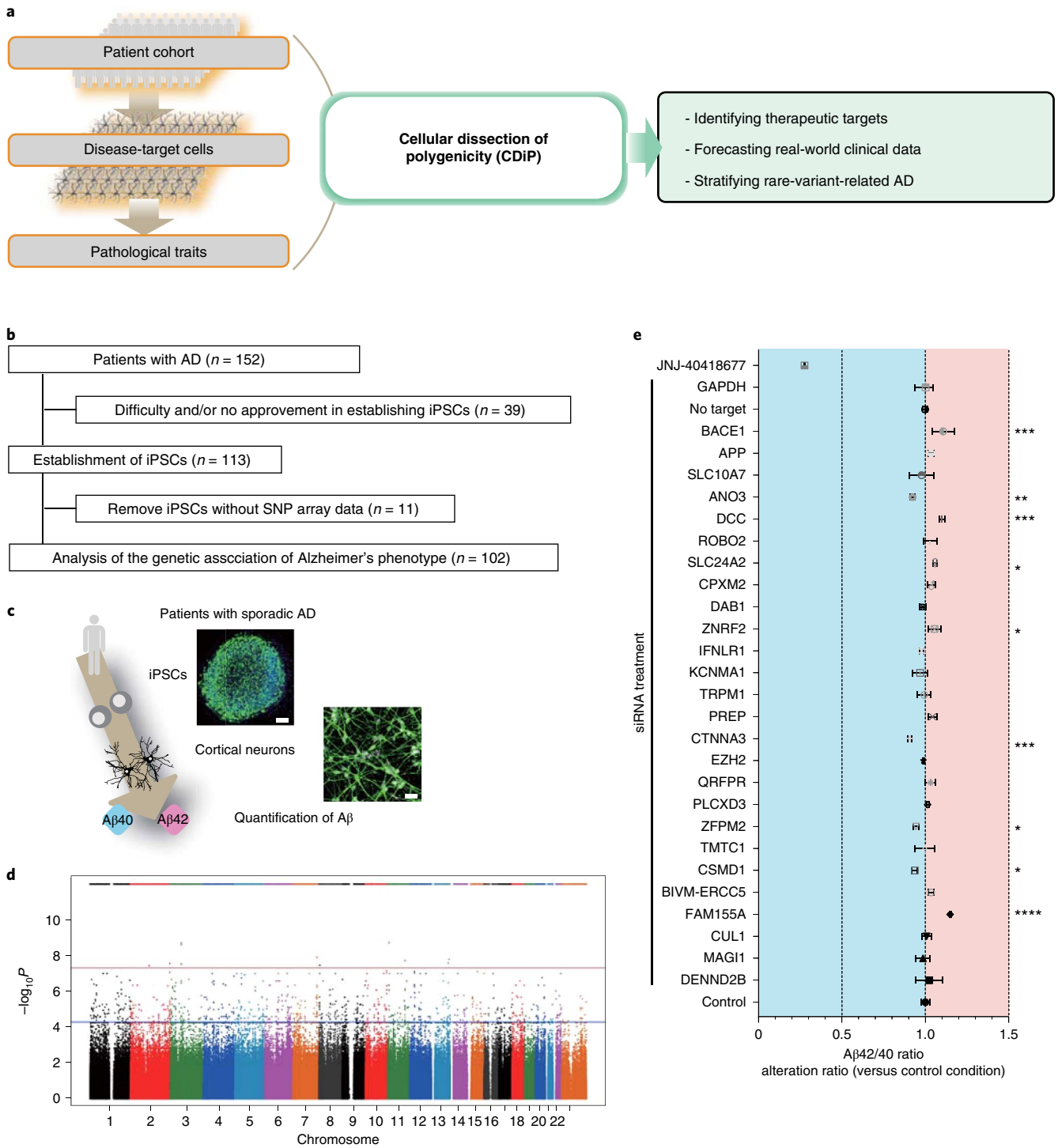

Fig. 1 | CDiP using induced cortical neurons from human iPSCs. a, Experimental design for polygenic analysis to investigate the correlation between genotype and disease phenotype in a cell-type-specific manner. **b**, Flowchart for patient enrollment and establishment of iPSCs. **c**, Variable Aβ phenotypes in cortical neurons differentiated from AD iPSC (representative images from three independent experiments for both iPSCs and neurons) cohort were quantified and compared among different patients with AD. Scale bars, 200 μm for iPSCs and 50 μm for cortical neurons. **d**, GWAS for CDiP was conducted to identify the genetic loci related to the Aβ42/40 ratio. Linear association between SNPs and the Aβ42/40 ratio was analyzed. Manhattan plot showing observed $-\log_{10} P$ of all tested SNPs with Aβ42/40 ratio (*y* axis). Chromosomes are presented on the *x* axis. The red line corresponds to a genome-wide Bonferroni-corrected significance threshold of $P < 5 \times 10^{-8}$. **e**, Knockdown of identified genes altered the Aβ42/40 ratio. Aβ phenotypes were analyzed after siRNA treatment, which targeted identified genes in CDiP, Aβ-related genes, including APP and BACE1. Non-target siRNA was used as a negative control. JNJ-40418677 1 μM, second generation of γ-secretase modulator to suppress Aβ42/40 ratio, was used as a positive control for altered Aβ phenotypes. The *x* axis shows the alteration level in Aβ42/40 ratio compared with the non-treatment control ($n = 2$ biological replicates). Shown is mean ± s.d. $^{*}P < 0.05$; $^{**}P < 0.01$; $^{***}P < 0.005$; $^{****}P < 0.001$ (one-way analysis of variance with uncorrected Fisher's least significant difference).

the number of neurons per well in different independent clones or patients (Extended Data Fig. 2a–d). To investigate the correlation with genomic information, we investigated the correlation of Aβ species with *APOE* genotypes (Extended Data Fig. 3a–d), which is the strongest genetic risk for AD. *APOE* ε4 genotypes were modestly correlated with the Aβ42/40 ratio (Extended Data Fig. 3c), as proven by other modalities[21–23] and was not correlated with the amount of Aβ (Extended Data Fig. 3a,b) nor protein concentration (Extended Data Fig. 3d). Previous reports using genetic modification techniques have also shown that *APOE4* alleles affect Aβ phenotypes of iPSC-derived neurons with an identical genetic background[24,25]. However, alteration of Aβ phenotypes in different SAD populations with APOE3/3 versus 4/4 (1.09-fold change in the present study) was less than that by genome-correction (approximately 1.2-fold or twofold change in previous reports) (Extended Data Fig. 3c). We also analyzed the correlation between quantified Aβ phenotypes in cortical neurons and clinical status, including onset age and sex. The amount of Aβ species and ratio were not correlated with onset age (Extended Data Fig. 4a–c) or sex (Extended Data Fig. 4d–f). These results indicate that Aβ phenotypes of SAD were affected by the diverse polygenic architecture of SAD. Therefore, we conducted a genome-wide investigation using Aβ in SAD cortical neurons for a pathological trait of AD.

To understand the polygenicity of Aβ, we conducted genome-wide analysis with the Aβ42/40 ratio in cortical neurons as a pathological trait (Extended Data Fig. 5a). Statistical analyses were adjusted for the *APOE* status and the false discovery rate for multiple testing was applied. The overall results did not show a large deviation from what was expected by chance ($\lambda = 0.9659$), meaning that there was no evidence for bias or inflation of our test statistics due to population stratification (Extended Data Fig. 5b). To estimate the effect of *APOE* genotypes, we conducted CDiP without adjustment for *APOE* genotypes at first (Extended Data Fig. 5c). As a result, the *P* value of rs429358 (T/C, locus of *APOE* ε4) was 0.794, which was not statistically significant. *APOE* ε4 has a strong risk for clinical AD, but CDiP showed that the Aβ42/40 ratio in a single-cell-type culture of iPSC-derived neurons is mainly affected by other complex gene sets than solely *APOE* ε4. Therefore, we conducted CDiP with adjustment for *APOE* genotypes and identified the genotypes of 24 single-nucleotide polymorphisms (SNPs) and related loci ($P < 5 \times 10^{-8}$ or loci containing >10 SNPs with $P < 5 \times 10^{-5}$), which are related to the altered Aβ42/40 ratio (Fig. 1d and Supplementary Table 2). The SNP with the highest genome-wide association was identified on chromosome 11 for rs34033747, an intronic SNP in DENN Domain Containing 2B (*DENND2B*) ($P = 1.91 \times 10^{-9}$) (Table 1). Five loci and related genes, including CUL1, QRFP, CTNNA3, DAB1 and DCC, were known to be associated with the Aβ production[26–31]. Further, eight loci and related genes, including MAGI1, TMTC1, TRPM1, KCNMA1, DAB1, CPXM2, ROBO2 and ANO3, have been reported as AD-related loci in clinical GWASs[32–36] or as clinical biomarkers[37–39]. Twelve loci and related genes were new as Aβ- or AD-related genes (Supplementary Table 3). In addition, most of the identified genes are expressed in the brain (Genotype-Tissue Expression (GTEx) portal, https://gtexportal.org/home/) and the expression patterns of 19 genes are highly expressed in neurons (Brain RNA-Seq portal, https://www.brainrnaseq.org/)[40] (Supplementary Table 3). Unbiased pathway analysis[41] identified 'calcium signaling pathway' as the top canonical pathway ($P = 2.51 \times 10^{-5}$) (Extended Data Fig. 5d). These networks are known to alter the Aβ metabolism[22,42]. These results proved that SNPs and related genes identified by the presented analysis of polygenic architecture contribute to the Aβ42/40 ratio and Alzheimer's pathology in cortical neurons as a cell-type-specific trait for AD pathology. In addition, as p231-tau, phosphorylated tau at threonine-231, is a sensitive marker for the diagnosis or tracing progression of AD[43,44], we quantified p231-tau/total tau ratio (p231-tau ratio) to apply p231-tau ratio to CDiP. *APOE* ε4 genotypes, sex and onset age of AD were not correlated with p231-tau ratio (Extended Data Fig. 6a–c). We conducted CDiP by using p231-tau ratio as the trait (Extended Data Fig. 6d,e) with or without adjustment for the *APOE* genotypes, we could determine the SNPs and related loci ($P < 5 \times 10^{-5}$) (Supplementary Tables 4 and 5). The lowest SNP *P* value was for rs6888116 ($P = 1.24 \times 10^{-6}$) at the TNFAIP8 locus, an inflammation-related molecule (Supplementary Table 4).

To prove the direct interaction between Aβ phenotype and the identified 24 genes in CDiP, we quantified Aβ species during knockdown of the identified genes (Fig. 1e and Extended Data Figs. 7a and 8a–c). When suppressing the expression of amyloid precursor protein (*APP*) or β-site APP cleaving enzyme 1 (*BACE1*), key components in Aβ production, the amounts of Aβ were decreased as expected (Extended Data Fig. 8a,b). Knockdown of 8 among 24 genes, identified in CDiP, significantly altered the Aβ42/40 ratio (Fig. 1e). Especially, we focused on *CTNNA3*, *ANO3* and *CSMD1*, which are the top three target genes with the largest reduction in Aβ42/40 ratio. Regarding the Aβ amount, knockdown of 23 among 24 genes, identified in CDiP, altered the amount of Aβ42 or Aβ40 (Extended Data Fig. 8a,b). Before selecting genes to focus on, we quantified the protein concentration after short interfering RNA (siRNA) treatment because the altered density of neurons must affect the amount of Aβ42. As a result, we found that knockdown of QRFPR, INFLR1, ZNRF2, ROBO2, DCC and APP reduced total protein concentration, as previously reported[31,45–47] (Extended Data Fig. 8c) and thus we excluded ZNRF2, INFLR1, DCC and APP from the latter interpretation for the altered amount of Aβ42. After that, we focused on *ZFPM2*, *TMTC1* and *KCNMA1*, which are the top three target genes with the largest reduction in the amount of Aβ42.

To narrow down the potential target of knockout therapy, we need to select genes whose expression is elevated in the neurons of AD brains. To examine the expression status of focused genes in AD neurons, we utilized the single-cell-based transcriptome data of the cortex of six AD brains and six control brains, which provide the transcriptome data for individual cell types, including neurons, astrocytes, oligodendrocyte progenitor cells, oligodendrocytes, microglia and endothelial cells[48]. We plotted the averaged expression of focused genes, including *CTNNA3*, *ANO3* and *CSMD1* for the Aβ42/40 ratio, *ZFPM2*, *TMTC1* and *KCNMA1* for Aβ42, specifically in neurons (Extended Data Fig. 8d,e) and found that expression of *CTNNA3*, *ANO3 and KCNMA1* was higher in AD brains. Taken together, we concluded that CTNNA3 and ANO3 for the Aβ42/40 ratio and KCNMA1 for the amount of Aβ42 could be potential therapeutic targets of AD (Extended Data Fig. 8f). The encoded protein of *CTNNA3* plays a role in cell–cell adhesion and mutation in *CTNNA3* causes familial arrhythmogenic right ventricular dysplasia[49], caused by mishandling of electrolytes such as potassium and calcium. The encoded protein of *KCNMA1* consists of voltage and calcium-sensitive potassium channels (KCa1.1) that regulate smooth muscle tone and neuronal excitability[50]. KCa1.1 is known as a target of cromolyn[51], notably having been tested in phase III trials for AD[52]. The encoded protein of *ANO3* is reported to have functions in endoplasmic reticulum-dependent calcium signaling and *ANO3* mutation causes familial dystonia type 24 via abnormal excitability of neurons[53]. From these results, identified therapeutic targets may be involved in calcium handling and excitability, an important pathway for Aβ modulation[42,54]. In summary, we dissected the complex cell types in AD into cortical neurons and conducted genome-wide analysis by setting neuron-specific Aβ and tau phenotypes as pathological traits of AD. As a result, CDiP revealed genotype sets partially contributing to the polygenic architecture behind the disease pathomechanism of AD.

Next, we assessed the analogy between in vitro datasets and real-world data consisting of positron emission tomography (PET)

Table 1 | List of identified SNPs and related loci, based on Aβ42/40 ratio in cortical neurons

Chr	position (bp)	dbSNP ID	β	s.e.m.	Minimum *P* value	Allele	Gene name	Gene ID
11	8853774	rs34033747	2.55×10^{-2}	3.84×10^{-3}	1.91×10^{-9}	C/T	*DENND2B* (*ST5*)	6764
3	65873820	rs58687721	1.92×10^{-2}	2.89×10^{-3}	1.97×10^{-9}	T/G	*MAGI1*	9223
7	148438804	rs11974639	1.57×10^{-2}	2.53×10^{-3}	1.26×10^{-8}	C/T	*CUL1*	8454
13	108015726	rs75174938	1.24×10^{-2}	2.01×10^{-3}	1.65×10^{-8}	G/A	*FAM155A*	728215
13	103486018	rs76029744	2.16×10^{-2}	3.57×10^{-3}	2.63×10^{-8}	A/T	*BIVM-ERCC5*	100533467
8	4801168	rs75778595	2.73×10^{-2}	4.55×10^{-3}	3.45×10^{-8}	G/A	*CSMD1*	64478
12	29790399	rs10843457	9.36×10^{-3}	1.61×10^{-3}	7.98×10^{-8}	T/C	*TMTC1*	83857
8	106566606	rs34823616	3.23×10^{-2}	5.62×10^{-3}	1.04×10^{-7}	T/C	*ZFPM2*	23414
5	41442044	rs318065	1.66×10^{-2}	2.96×10^{-3}	1.80×10^{-7}	T/C	*PLCXD3*	345557
4	122249973	rs6821123	2.55×10^{-2}	4.68×10^{-3}	3.98×10^{-7}	C/T	*QRFPR*	84109
7	148530294	rs10245290	1.78×10^{-2}	3.30×10^{-3}	4.85×10^{-7}	T/C	*EZH2*	2146
10	67784976	rs10996833	2.47×10^{-2}	4.70×10^{-3}	8.74×10^{-7}	A/G	*CTNNA3*	29119
6	105721926	rs72938040	2.43×10^{-2}	4.75×10^{-3}	1.66×10^{-6}	A/G	*PREP*	5550
15	31294343	rs12898290	2.91×10^{-2}	5.77×10^{-3}	2.19×10^{-6}	A/T	*TRPM1*	4308
10	78859025	rs80058374	7.81×10^{-3}	1.57×10^{-3}	2.78×10^{-6}	T/C	*KCNMA1*	3778
1	24495722	rs4649197	9.86×10^{-3}	2.03×10^{-3}	4.76×10^{-6}	A/G	*IFNLR1*	163702
7	30370786	rs11974360	1.08×10^{-2}	2.23×10^{-3}	5.12×10^{-6}	A/G	*ZNRF2*	223082
1	58715824	rs117567026	1.52×10^{-2}	3.20×10^{-3}	6.69×10^{-6}	C/G	*DAB1*	1600
10	125679317	rs72631124	1.35×10^{-2}	2.92×10^{-3}	1.09×10^{-5}	G/A	*CPXM2*	119587
9	19642563	rs16937677	9.40×10^{-3}	2.05×10^{-3}	1.36×10^{-5}	G/A	*SLC24A2*	25769
3	77035984	rs67172613	1.73×10^{-2}	3.80×10^{-3}	1.60×10^{-5}	T/C	*ROBO2*	6092
18	50295649	rs28592006	1.17×10^{-2}	2.62×10^{-3}	2.12×10^{-5}	C/G	*DCC*	1630
11	26600213	rs61877058	2.20×10^{-2}	4.93×10^{-3}	2.14×10^{-5}	G/A	*ANO3*	63982
4	147199809	rs60367087	2.13×10^{-2}	4.87×10^{-3}	3.15×10^{-5}	C/T	*SLC10A7*	84068

Chr, chromosome; dbSNP ID, dbSNP accession code; allele, reference allele/minor allele; gene ID, NCBI Gene identifier

imaging for brain Aβ deposition of patients who provided the peripheral blood mononuclear cells (PBMCs) for iPSC establishment in this study. We analyzed the correlation between quantified Aβ phenotypes in cortical neurons and brain Aβ deposition as measured by Pittsburgh Compound-B (PiB)-PET imaging[55,56] (Extended Data Fig. 9a). However, neither age at onset nor Aβ phenotypes were correlated with brain Aβ deposition (Extended Data Fig. 9b–e). From these facts we confirmed that the simple quantified disease phenotypes without genetic information could not reflect real-world data. Therefore, we examined whether, by using these genotype sets, we could predict real-word big data from independent AD cohorts. We utilized the database of the Alzheimer's Disease Neuroimaging Initiative (ADNI)[57–59], including genome-wide genotypes, brain Aβ deposition (AV45-PET), CSF Aβ42, CSF total tau (t-tau) and CSF phosphorylated tau (p-tau). First, we attempted to predict the positivity of brain Aβ deposition by using only covariates consisting of age, sex, genotype of *APOE*-ε4 allele or covariates plus genotype sets. We established machine-learning models to predict the positivity of brain Aβ deposition by using only covariates consisting of age, sex, genotype of *APOE*-ε4 allele or covariates plus identified genotype sets. By using trained models, we attempted to predict brain Aβ and compared the area under the curve (AUC) between two different models. The AUC by covariates plus genotype sets (AUC = 0.76) was statistically higher than that for only covariates (AUC = 0.66) (Fig. 2a). Similarly, covariates plus genotype sets could predict the decrease in CSF Aβ42 with significantly higher accuracy compared to only covariates (Fig. 2b). However, when predicting CSF t-tau or CSF p-tau, there was no significant difference between the AUCs of covariates and covariates plus genotype sets (Fig. 2c,d). Collectively, with the genotype sets identified by CDiP, we could predict real-world clinical data of AD.

To confirm the further applicability of the system to real-world clinical data, we examined whether the identified gene sets shaped SAD. We examined the relevance of the genes identified in the current study as rare variants, which are known to be low frequency but minor factors in the development of AD. We examined the rare variants in the identified loci using genome-wide exome data from the J-ADNI[60] (Extended Data Fig. 9f). We investigated the rare variants in 24 gene loci, in association with the Aβ42/40 ratio, by investigating exome data from healthy donors ($n = 152$) and patients with SAD ($n = 255$). Rare variants in *KCNMA1* ($P = 0.032$; odds ratio (OR), 1.45) showed a relationship with AD (Supplementary Table 6 and Supplementary Data 1). To confirm the reproducibility of rare variants in different cohorts and different ethnicities, we conducted a meta-analysis to investigate rare variants in 24 gene loci and we identified rare variants in *KCNMA1* loci ($P = 0.010$; OR, 1.49) again (Table 2 and Supplementary Data 1 and 2) by meta-analysis of J-ADNI and ADNI (Extended Data Fig. 9f). These results indicate that identified gene sets are applicable for elucidating predisposing factors for the development of SAD.

In the current research, risk SNPs, genes in which SNPs locate and molecular pathways affecting the Aβ production in cortical neurons were identified. In fact, 5 of the 24 genes, namely *TMTC1*, *CTNNA3*, *KCNMA1*, *CPXM2* and *ANO3*, identified by CDiP, were consistent with the reported results of a clinical genome-wide study, which is based on clinical data, with disease onset or brain Aβ deposition (summarized in Supplementary Table 3). This advantage may stem from the fact that we used a homogeneous population of

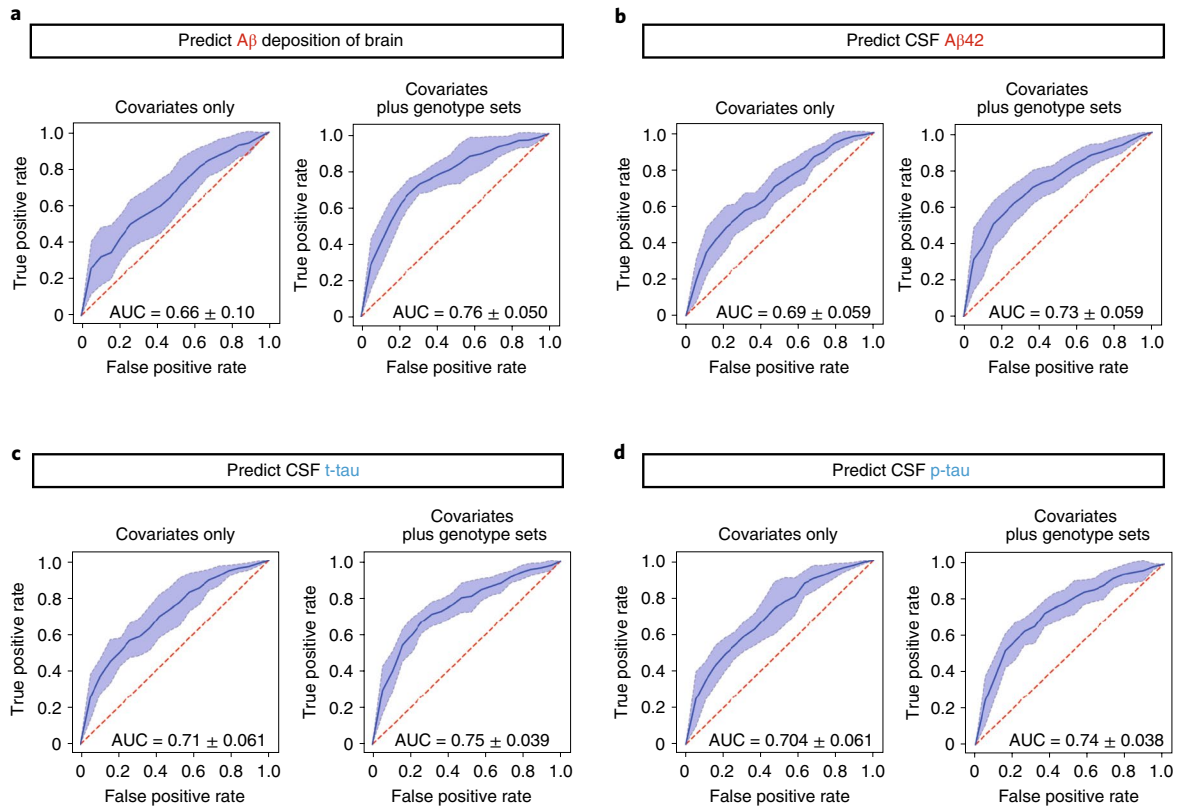

Fig. 2 | Genotype sets identified by CDiP can be a key clue for predicting real-world data of Alzheimer's cohort with genetic risk for AD. a, Clinical phenotypes of the ADNI database were classified as AD-like condition positive or negative and were predicted using covariates (age, sex, genotype of APOE-ε4 allele) or covariates plus genotype sets, identified in CDiP. In the case of brain Aβ deposition examined by AV45-PET, the AUCs predicted by covariates plus genotype sets (right) were significantly higher than the AUCs predicted by covariates only (left) (paired Student's *t*-test $P < 0.05$). **b**, In the case of CSF Aβ (1–42), the AUCs predicted by covariates plus genotype sets (right) were significantly higher than the AUCs predicted by covariates only (left) (paired Student's *t*-test $P < 0.05$). **c**, In case of CSF t-tau, AUCs predicted by covariates plus genotype sets (right) were higher than those predicted by only covariates (left), but the difference was not statistically significant. **d**, In the case of CSF p-tau, AUCs predicted by covariates plus genotype sets (right) were higher than those predicted by only covariates (left), but the difference was not statistically significant.

cortical neurons, a main cell type serving as resources for Aβ production. The genes (Table 1) newly identified in this study may play a pivotal role in AD pathogenesis as well as represent potential biomarkers and candidates for therapeutic targets.

To expand the presented systems, other kinds of neuronal phenotypes in AD pathology may be applicable to CDiP to identify the genetic background specific to each trait, such as synaptic loss, neuronal death, drug response and vulnerability to environmental stresses. In addition, new combinations of variable cell types such as glial cells[61] and cell-type-specific pathologies will uncover new genetic architecture of molecular pathology, which was masked in clinical GWASs[2]. In recent research, the concept that AD is the summation of pathologies in diverse cell types has been emphasized. Based on ideas similar to the present study, single-nucleus transcriptomes from autopsied AD brains provided the information regarding gene expression for different cell types[48,62,63]. However, such an approach based on autopsied brain samples can take a snapshot of the end stage in AD pathology, which had continued to change for decades. In contrast, CDiP can investigate the separated AD pathology with cell-type specificity and also model the baseline state without confounding factors, which can be a noise in genome-wide studies.

The limitation of CDiP is that CDiP is based on a two-dimensional monolayer culture consisting of a single cell type. To understand the cellular interaction among various cell types, the combination of CDiP and single-nucleus transcriptomes from autopsy brains of patients with AD may be two of the most important tools to investigate the polygenicity of AD as presented in this study (Extended Data Fig. 8d–f). In addition, CDiP with neurons identified rare variants and potential therapeutic targets associated with Aβ phenotypes. On the other hand, SNPs associated with tau phenotypes showed more moderate statistically significant correlations. This difference between Aβ and tau indicated that Aβ pathology is mainly based on the polygenicity of neurons, whereas tau pathology might consist of multiple type of cells other than solely neurons. In fact, previous reports showed that inflammatory conditions and brain networks with microglia and astrocytes accelerate tau pathology[64–66]. Furthermore, there is clinical evidence suggesting that APOE regulates tau pathology independently of Aβ pathology[67]. CDiP with neurons may suggest one aspect of discontinuity between Aβ and tau pathology (Extended Data Fig. 10a). In the future, it is hoped that an integrated and comprehensive understanding of the genetic background obtained by these cell-type-specific analytical approaches will lead to a better understanding of the complex pathogenesis of AD.

In this study using CDiP we predicted AD real-world data, stratified rare-variant-related AD and identified CTNNA3, ANO3 and KCNMA1 as potential therapeutic targets. CDiP is useful as a screening tool for linking pathological phenotypes with hidden genotypes. On the other hand, it is also important to accumulate evidence using different modalities such as mouse models and patient specimens for adaptation to real AD pathology, which is composed

Table 2 | Investigation of rare variants in gene loci by using ADNI data

Chr	Gene	*P*	*β*	s.e.m.	cmafTotal	cmafUsed	nsnpsTotal	nsnpsUsed	nmiss	OR	s.e.m.
1	*DAB1*	0.223	−0.75	0.61	0.012	0.012	9	9	3,879	0.47	1.85
1	*IFNLR1*	0.344	0.44	0.47	0.024	0.024	13	13	5,867	1.55	1.59
3	*MAGI1*	0.668	−0.08	0.19	0.078	0.078	36	36	14,007	0.92	1.21
3	*ROBO2*	0.649	−0.13	0.28	0.052	0.052	25	25	10,463	0.88	1.33
4	*QRFPR*	0.389	−0.18	0.21	0.059	0.059	21	21	9,195	0.83	1.24
4	*SLC10A7*	0.840	−0.11	0.53	0.017	0.017	13	13	5,507	0.90	1.70
5	*PLCXD3*	0.145	−2.06	1.42	0.002	0.002	4	4	1,772	0.13	4.13
6	*PREP*	0.800	0.14	0.56	0.017	0.017	13	13	5,867	1.15	1.75
7	*CUL1*	0.513	−0.09	0.14	0.046	0.046	11	11	4,981	0.91	1.16
7	*EZH2*	0.215	0.85	0.68	0.010	0.010	6	6	2,586	2.33	1.98
7	*ZNRF2*	0.233	0.51	0.43	0.025	0.025	6	6	2,514	1.66	1.53
8	*CSMD1*	0.187	0.18	0.14	0.224	0.224	111	111	46,836	1.20	1.15
8	*ZFPM2*	0.242	0.31	0.26	0.064	0.064	29	29	11,900	1.36	1.30
9	*SLC24A2*	0.917	0.03	0.29	0.049	0.049	21	21	8,572	1.03	1.33
10	*CPXM2*	0.218	−0.39	0.32	0.040	0.040	25	25	10,823	0.68	1.37
10	*CTNNA3*	0.932	0.02	0.26	0.065	0.065	33	33	14,295	1.02	1.30
10	*KCNMA1*	0.010	0.40	0.16	0.093	0.093	38	38	14,007	1.49	1.17
11	*ANO3*	0.327	0.29	0.30	0.050	0.050	23	23	10,153	1.34	1.34
11	*DENND2B*	0.098	−0.40	0.24	0.081	0.081	22	22	9,962	0.67	1.28
12	*TMTC1*	0.954	0.02	0.28	0.054	0.054	23	23	10,009	1.02	1.33
13	*BIVM-ERCC5*	0.207	−0.34	0.27	0.053	0.053	41	41	16,114	0.71	1.31
13	*FAM155A*	0.481	0.26	0.37	0.031	0.031	9	9	3,879	1.30	1.45
15	*TRPM1*	0.070	0.30	0.17	0.143	0.143	55	55	23,537	1.35	1.18
18	*DCC*	0.460	−0.11	0.15	0.207	0.207	53	53	23,299	0.89	1.17

P, *P* value from the burden tests; s.e.m., approximate standard error for the effect of genotype; cmafTotal, the cumulative minor allele frequency of the gene; mafUsed, the cumulative minor allele frequency of SNPs used in the analysis; nsnpsTotal, the number of SNPs in the gene; nsnpsUsed, the number of SNPs used in the analysis; nmiss, the number of 'missing' SNPs. For a gene with a single SNP this is the number of individuals who do not contribute to the analysis due to studies that did not report results for that SNP. For a gene with multiple SNPs, values are totaled over the gene.

of various cell types and is also completed over a period of decades. CDiP will provide a key to understanding a complex pathology as a sum of polygenicity in disease-target cells and traits, paving the way toward precision medicine.

Methods

Patient cohort and establishment of iPSCs. The present study was approved by the Ethics Committee of the Center for iPS Cell Research and Application, Kyoto University (approval nos. CiRA19-05 and CiRA20-14). For the establishment of iPSCs from human PBMCs, PBMCs of patients with AD were collected according to the research project, which was approved by the Ethics Committee of the Department of Medicine and Graduate School of Medicine, Kyoto University (approval nos. R0091, G259 and G0722). Written, informed consent was obtained from all participants in this study. Human complementary DNA for reprogramming factors was transduced in human PBMCs with episomal vectors (SOX2, KLF4, OCT4, L-MYC, LIN28 and dominant negative p53). Several days after transduction, PBMCs were collected and replated on dishes coated with laminin 511-E8 fragment (iMatrix 511, Nippi). The medium was changed to StemFit AK03 the next day. Following that, the medium was changed every second day. Twenty days after transduction, iPSC colonies were picked up. Established PBMC-origin iPSCs were expanded for neural differentiation.

Induced cortical neurons from human iPSCs. We utilized a direct conversion technology to establish a robust, quick differentiation method. Human neurogenin2 (*NGN2*) cDNA, under tetracycline-inducible promoter (tetO), was transfected into iPSCs by a *piggyBac* transposon system and Lipofectamine LTX (Thermo Fisher Scientific). We used the vector containing tetO::NGN2. After antibiotic selection of G418 disulfate (Nacalai Tesque), we picked out colonies and selected subclones that could efficiently differentiate into neurons by inducing the temporal expression of NGN2, with MAP2/4,6-diamidino-2-phenylindole at 96% purity.

Karyotyping and genotyping. Karyotyping was performed by LSI Medience (Tokyo, Japan). Genotyping of single-nucleotide mutation was performed by PCR amplification of genomic DNA and directly sequenced (3100 Genetic Analyzer; Thermo Fisher). The *APOE* gene was amplified by PCR (forward primer TCCAAGGAGCTGCAGGCGGCGCA; reverse primer ACAGAATTCGCCCCGGCCTGGTACACTG). PCR products were digested by HhaI at 37 °C for 2 h and then subjected to electrophoresis to analyze the band size.

Quantitative PCR of XIST expression. Total RNA was purified from human iPSCs or human embryonic stem cells H9 clone by using RNAeasy kit (QIAGEN) and was reverse transcribed by using RevaTra Ace kit (Toyobo). Quantitative PCR (qPCR) was conducted by using the SYBR Green PCR kit (Takara) and QuantStudio5 (Thermo Fisher) following the manufacturer's instructions. Results were normalized to *ACTB* and *XIST* expression was calculated by the $2^{-\Delta\Delta Ct}$ method. The sequence of qPCR primers was (forward) AGAGCTACGAGCTGCCTGAC and (reverse) CGTGGATGCCACAGGACT for *ACTB* and (forward) AGCTCCTCGGACAGCTGTAA and (reverse) CTCCAGATAGCTGGCAACC for *XIST*[12].

Immunocytochemistry. Cells were fixed in 4% paraformaldehyde (pH 7.4) at room temperature and were permeabilized in PBST containing 0.2% Triton X-100. Nonspecific binding was blocked with BlockingONE histo (Nacalai Tesque) for 60 min at room temperature[13]. Cells were incubated with primary antibodies overnight at 4 °C and then labeled with fluorescent-tagged secondary antibodies. Nuclei were labeled with 4,6-diamidino-2-phenylindole (Thermo Fisher). Images of cells were acquired on high-content confocal microscope IN Cell analyzer 6000 (GE Healthcare). We used the following primary antibodies for immunocytochemistry: NANOG (1:100 dilution, Abcam ab80892), TRA1-60 (1:400 dilution, CST 4746), MAP2 (1:4,000 dilution, Abcam ab5392), SATB2 (1:400 dilution, Abcam ab92446), Alexa 488-conjucated antibody (1:400 dilution, Thermo Fisher, A11029), Alexa 488-conjucated antibody (1:400 dilution, Thermo Fisher, A11039) and Alexa 594-conjucated antibody (1:400 dilution, Thermo Fisher, A21207).

Quantification of protein concentration. On day 10, the RIPA-soluble fraction of total protein was extracted from differentiated neurons, cultivated in 96-well plates by the addition of 30 µl RIPA buffer and centrifuged at 12,000*g* for 30 min to collect

supernatant. The protein concentration of the supernatant was measured with a Pierce BCA protein assay kit (Thermo Fisher) by following the kit manual.

Pathway analysis for identified gene. We performed pathway analysis of the 230 identified genes ($P<5\times10^{-5}$) using commercial Ingenuity Pathway Analysis (QIAGEN, https://www.qiagenbioinformatics.com/) software and analyzed the top networks.

Electrochemiluminescence assays for Aβ. All culture medium was replaced with 100 µl of fresh medium on day 8. Conditioned medium was collected for further analysis on day 10. Aβ species in culture medium were measured by human (6E10) Aβ 3-Plex kit (Meso Scale Discovery) for extracellular human Aβ. For Aβ species, this assay uses 6E10 antibody to capture Aβ peptide and SULFO-TAG-labeled different C-terminal-specific anti-Aβ antibodies for detection by electrochemiluminescence with Sector Imager 2400 (Meso Scale Discovery). Quantified Aβ values ($n=2$ wells per clone) were adjusted using total protein concentration of neurons to compare among conditions by minimizing the noise originating from the altered cell number.

Electrochemiluminescence assays for tau protein. Tau species in RIPA lysate extracted from iPSC-derived neurons were measured by Phospho(Thr231)/Total Tau kit (Meso Scale Discovery) according to the kit instructions. Quantified tau values ($n=2$ wells per clone) were adjusted using the total protein concentration of neurons to compare among conditions by minimizing the noise originating from the altered cell number.

SNP genotyping of patients with AD and GWAS for cellular dissection of polygenicity. All 102 PBMC samples from patients with AD were genotyped with Infinium OmniExpressExome-8 v.1.4 BeadChip according to the kit manual (Illumina). To isolate algorithmic issues from data format issues, we standardized all genotype data to forward strand GRCh37.p13 orientation as is generated by variant calling from whole-genome sequencing data. After genotyping by using GenomeStudio (Illumina) and quality control (Hardy–Weinberg equilibrium, $P>1.0\times10^{-6}$; minor allele frequency ≥0.01; linkage disequilibrium-based variant pruning $r^2<0.8$; window size, 100 kb; step size, 5), the genotypes were imputed with minimac4 using 1000 Genomes Project Phase 3 as a reference panel. Overall, 7,349,481 SNPs passed the post-imputation quality threshold ($r^2\geq0.3$, minor allele frequency ≥0.01). Linear association between SNPs and the Aβ42/40 ratio accumulation ratio in iPSC-derived neurons was analyzed with plink 1.9, where onset age, sex and genotype of the *APOE*-ε4 allele were included as covariates in linear regression models. $P<5\times10^{-5}$ was set as the suggested level and $P<5\times10^{-8}$ as the significant level of the association analysis. No statistical methods were used to predetermine sample sizes but our sample sizes were similar to those reported in previous publications[68].

Prediction of clinical data in ADNI datasets. The results of the Aβ 42/40 ratio in cortical neurons were processed through LD-based clumping ($r^2>0.2$; window size, 1 Mb) with plink 1.9. Among independent SNPs, those above the suggested threshold level ($P<5\times10^{-5}$) in genome-wide analysis were 496 SNPs, which were used as variables of a prediction model. A selected SNP genotype matrix of 102 samples from patients with AD, the elements of which originally consisted of 0, 1 or 2, was normalized and analyzed by principal-component analysis. Genotypes of samples from the ADNI 1/GO/2 datasets were collected (Illumina; Omni 2.5M BeadChip). Quality control and imputation were performed on the genotype data under the same conditions. The imputed genotypes of 10,121,962 SNPs were filtered by genome-wide analysis-derived 496 SNPs. The genotypes of SNPs that were listed in a CDiP list but not in ADNI datasets were complemented with the mean genotypes of inhouse patients with AD. Then, phenotypes of ADNI samples were predicted from genotypes. We predicted whether a sample belonged to an AD-like condition (positive) or not (negative). Samples were categorized as positive or negative independently according to four criteria based on reported results in the ADNI database: (1) the standardized uptake value ratio (reference, cerebellar reference region) from AV45-PET data (>1.1, a threshold for positive); (2) Aβ(1–42) in CSF (<977 pg ml^{-1}, a threshold for positive);[69] (3) t-tau/Aβ(1–42) in CSF (>0.27, a threshold for positive); and (4) p-tau/Aβ(1–42) in CSF (>0.025, a threshold for positive)[69]. All reported results were obtained from the ADNIMERGE dataset at baseline. Samples with both genotype data and phenotype data were included in the study (standardized uptake value ratio AV45; $N=512$; CSF Aβ(1–42), t-t-tau/Aβ(1–42), p-tau/Aβ(1–42); $N=581$). Genotype vectors of ADNI samples were mapped to the principal-component space derived from the genotype matrix of inhouse patients with AD. We performed tenfold cross validation. ADNI samples were split into training samples and test samples. A random forest classifier (100 estimators) was trained with the training samples, where target variables (AD-like condition positive/negative) were predicted from the top three principal components in the genotype matrix and covariates (age, sex, genotype of *APOE*-ε4 allele). The performance of prediction was evaluated with AUC of receiver operating characteristics curve results from prediction in test samples. The prediction performance was compared to the case when target variables were predicted only from covariates. Significance of AUC improvement was tested with a Wilcoxon signed-rank test (significant threshold, $P<0.05$).

Knockdown of target genes. Cells at an initial density of 3,000,000 cells per well of six-well plates were disseminated on day 5. At 24 h after dissemination (day 6), culture medium was replaced with neurobasal medium containing 1 µM Accell SMARTpool siRNA (Horizon Discovery). We cultivated iPSC-derived neurons for 72 h from days 6 to 9 to maximize the Accell siRNA effect. At 72 h after adding siRNA (day 9), culture medium was refreshed with neurobasal medium containing fresh 1 µM Accell SMARTpool siRNA or 1 µM JNJ-40418677 (Sigma-Aldrich) and collection was performed on day 11 to analyze the Aβ phenotypes.

Investigation for rare variants related to AD onset. Whole-exome sequencing was performed on 407 blood-derived genomic DNA samples obtained from 255 patients with AD and 152 cognitively healthy controls participating in the J-ADNI project[60]. Exonic sequences were enriched via hybridization using Agilent's SureSelect Human All Exon kit (V6) and sequenced on Illumina HiSeq4000 using paired-end read chemistry. Short-read sequences in the target region were mapped to the human reference genome (hg38) using BWA-MEM v.0.7.15-r1140 with default settings. The subsequent analyses (read processing, variant calling and variant filtration) were conducted according to GATK4 Best Practices recommendation[70], followed by variant annotation using snpEff v.4.3t. Among all variants identified by whole-exome sequencing, we focused on nonsynonymous, nonsense, splice-site, insertion or deletion variants. We further narrowed this down to variants with mean allele frequency <0.05 in publicly available databases using the publicly available databases ExAC (release 0.3; http://exac.broadinstitute.org/), gnomAD (release 2.1.1 for exomes and r.3.0 for genomes; https://gnomad.broadinstitute.org/), HGVD v.2.3 (http://www.hgvd.genome.med.kyoto-u.ac.jp/) and ToMMo v.8.3KJPN (https://jmorp.megabank.tohoku.ac.jp). A gene-based association study of the variants was performed using a burden test[47] on an R package seqMeta v.1.6.7 using J-ADNI ($N=407$) and ADNI ($N=479$) exome data.

Statistics and reproducibility. Except for prediction of clinical data in ADNI datasets and investigation of rare variants related to AD onset, we conducted statistical analysis as below. All data are shown as mean ± s.d. We conducted two or three experimental replicates to confirm reproducibility. Data distribution was assumed to be normal but this was not formally tested. Comparisons of mean among three groups or more were performed by one-way analysis of variance followed by a post hoc test using Tukey's multiple comparisons test or uncorrected Fisher's least significant difference test (GraphPad Prism 7.0 software (GraphPad)). P values <0.05 were considered significant.

Reporting Summary. Further information on research design is available in the Nature Research Reporting Summary linked to this article.

Data availability

Data used in the preparation of this article were obtained from the ADNI database (adni.loni.usc.edu). ADNI was launched in 2003 as a public–private partnership, led by principal investigator M.W.W.. The primary goal of ADNI has been to test whether serial magnetic resonance imaging, PET, other biological markers and clinical and neuropsychological assessments can be combined to measure progression of mild cognitive impairment and early AD. SNP array data are available in the National Bioscience Database Center (data ID hum031; JGAS000383/JGAD00049). All data generated or analyzed during this study are included in this article and its Supplementary Information files.

Code availability

All code for data management and analysis is archived online at GitHub (https://github.com/HaruhisaInoue/iSNPs4ADNIpred). All other codes as described above are openly available in the developer site.

Received: 4 December 2020; Accepted: 23 November 2021;
Published online: 17 February 2022

References

1. Gatz, M. et al. Role of genes and environments for explaining Alzheimer disease. *Arch. Gen. Psychiatry* **63**, 168–174 (2006).
2. Andrews, S. J., Fulton-Howard, B. & Goate, A. Interpretation of risk loci from genome-wide association studies of Alzheimer's disease. *Lancet Neurol.* **19**, 326–335 (2020).
3. Sims, R., Hill, M. & Williams, J. The multiplex model of the genetics of Alzheimer's disease. *Nat. Neurosci.* **23**, 311–322 (2020).
4. Dou, K. X. et al. Genome-wide association study identifies CBFA2T3 affecting the rate of CSF Aβ42 decline in non-demented elders. *Aging* **11**, 5433–5444 (2019).
5. Hong, S. et al. Genome-wide association study of Alzheimer's disease CSF biomarkers in the EMIF-AD Multimodal Biomarker Discovery dataset. *Transl. Psychiatry* https://doi.org/10.1038/s41398-020-01074-z (2020).
6. Liu, C. & Yu, J. Genome-wide association studies for cerebrospinal fluid soluble TREM2 in Alzheimer's disease. *Front. Aging Neurosci.* https://doi.org/10.3389/fnagi.2019.00297 (2019).

7. Deming, Y. et al. Genome-wide association study identifies four novel loci associated with Alzheimer's endophenotypes and disease modifiers. *Acta Neuropathol.* **133**, 839–856 (2017).
8. Kim, S. et al. Genome-wide association study of CSF biomarkers Aβ1-42, t-tau, and p-tau181p in the ADNI cohort. *Neurology* **76**, 69–79 (2011).
9. Han, M. R., Schellenberg, G. D. & Wang, L. S. Genome-wide association reveals genetic effects on human Aβ42and τ protein levels in cerebrospinal fluids: a case control study. *BMC Neurol.* https://doi.org/10.1186/1471-2377-10-90 (2010).
10. Tam, V. et al. Benefits and limitations of genome-wide association studies. *Nat. Rev. Genet.* **20**, 467–484 (2019).
11. Gallagher, M. D. & Chen-Plotkin, A. S. The post-GWAS era: from association to function. *Am. J. Hum. Genet.* **102**, 717–730 (2018).
12. Hoffman, L. M. et al. X-inactivation status varies in human embryonic stem cell lines. *Stem Cells* **23**, 1468–1478 (2005).
13. Kondo, T. et al. iPSC-based compound screening and in vitro trials identify a synergistic anti-amyloid β combination for Alzheimer's disease. *Cell Rep.* **21**, 2304–2312 (2017).
14. Hardy, J. & Selkoe, D. J. The amyloid hypothesis of Alzheimer's disease: progress and problems on the road to therapeutics. *Science* **297**, 353–356 (2002).
15. Selkoe, D. J. Alzheimer's disease is a synaptic failure. *Science* **298**, 789–791 (2002).
16. Gadadhar, A., Marr, R. & Lazarov, O. Presenilin-1 regulates neural progenitor cell differentiation in the adult brain. *J. Neurosci.* **31**, 2615–2623 (2011).
17. Porayette, P. et al. Differential processing of amyloid-β precursor protein directs human embryonic stem cell proliferation and differentiation into neuronal precursor cells. *J. Biol. Chem.* **284**, 23806–23817 (2009).
18. Araki, W. et al. Trophic effect of β-amyloid precursor protein on cerebral cortical neurons in culture. *Biochem. Biophys. Res. Commun.* **181**, 265–271 (1991).
19. Freude, K. K., Penjwini, M., Davis, J. L., LaFerla, F. M. & Blurton-Jones, M. Soluble amyloid precursor protein induces rapid neural differentiation of human embryonic stem cells. *J. Biol. Chem.* **286**, 24264–24274 (2011).
20. Arber, C. et al. Familial Alzheimer's disease mutations in PSEN1 lead to premature human stem cell neurogenesis. *Cell Rep*. https://doi.org/10.1016/j.celrep.2020.108615 (2021).
21. Jan, A., Gokce, O., Luthi-Carter, R. & Lashuel, H. A. The ratio of monomeric to aggregated forms of Aβ40 and Aβ42 is an important determinant of amyloid-β aggregation, fibrillogenesis, and toxicity. *J. Biol. Chem.* **283**, 28176–28189 (2008).
22. Zoltowska, K. M., Maesako, M. & Berezovska, O. Interrelationship between changes in the amyloid β 42/40 ratio and presenilin 1 conformation. *Mol. Med.* **22**, 329–337 (2016).
23. Kwak, S. S. et al. Amyloid-β42/40 ratio drives tau pathology in 3D human neural cell culture models of Alzheimer's disease. *Nat. Commun*. https://doi.org/10.1038/s41467-020-15120-3 (2020).
24. Wang, C. et al. Gain of toxic apolipoprotein E4 effects in human iPSC-derived neurons is ameliorated by a small-molecule structure corrector. *Nat. Med.* **24**, 647–657 (2018).
25. Lin, Y.-T. et al. APOE4 causes widespread molecular and cellular alterations associated with Alzheimer's disease phenotypes in human iPSC-derived brain cell types. *Neuron* **98**, 1141–1154 (2018).
26. Yasukawa, T. et al. NRBP1-containing CRL2/CRL4A regulates amyloid β production by targeting BRI2 and BRI3 for degradation. *Cell Rep.* **30**, 3478–3491 (2020).
27. Davies, J. et al. Orexin receptors exert a neuroprotective effect in Alzheimer's disease (AD) via heterodimerization with GPR103. *Sci. Rep*. https://doi.org/10.1038/srep12584 (2015).
28. Ertekin-Taner, N. et al. Linkage of plasma Aβ42 to a quantitative locus on chromosome 10 in late-onset Alzheimer's disease pedigrees. *Science* **290**, 2303–2304 (2000).
29. Hoe, H. S., Tran, T. S., Matsuoka, Y., Howell, B. W. & Rebeck, G. W. DAB1 and reelin effects on amyloid precursor protein and ApoE receptor 2 trafficking and processing. *J. Biol. Chem.* **281**, 35176–35185 (2006).
30. Hoe, H. S. et al. Fyn modulation of Dab1 effects on amyloid precursor protein and apoe receptor 2 processing. *J. Biol. Chem.* **283**, 6288–6299 (2008).
31. Lourenço, F. C. et al. Netrin-1 interacts with amyloid precursor protein and regulates amyloid-β production. *Cell Death Differ.* **16**, 655–663 (2009).
32. Rovelet-Lecrux, A. et al. A genome-wide study reveals rare CNVs exclusive to extreme phenotypes of Alzheimer disease. *Eur. J. Hum. Genet.* **20**, 613–617 (2012).
33. Logue, M. W. et al. A comprehensive genetic association study of Alzheimer disease in African Americans. *Arch. Neurol.* **68**, 1569–1579 (2011).
34. Beecham, G. W. et al. Genome-wide association study implicates a chromosome 12 risk locus for late-onset Alzheimer disease. *Am. J. Hum. Genet.* **84**, 35–43 (2009).
35. Chen, Y. C. et al. Performance metrics for selecting single nucleotide polymorphisms in late-onset Alzheimer's disease. *Sci. Rep*. https://doi.org/10.1038/srep36155 (2016).
36. Kunkle, B. W. et al. Genetic meta-analysis of diagnosed Alzheimer's disease identifies new risk loci and implicates Aβ, tau, immunity and lipid processing. *Nat. Genet.* **51**, 414–430 (2019).
37. Scelsi, M. A. et al. Genetic study of multimodal imaging Alzheimer's disease progression score implicates novel loci. *Brain* **141**, 2167–2180 (2018).
38. Whelan, C. D. et al. Multiplex proteomics identifies novel CSF and plasma biomarkers of early Alzheimer's disease. *Acta Neuropathol. Commun*. https://doi.org/10.1186/s40478-019-0795-2 (2019).
39. Jiang, S. et al. A systems view of the differences between APOE ε4 carriers and non-carriers in Alzheimer's disease. *Front. Aging Neurosci*. https://doi.org/10.3389/fnagi.2016.00171 (2016).
40. Zhang, Y. et al. Purification and characterization of progenitor and mature human astrocytes reveals transcriptional and functional differences with mouse. *Neuron* **89**, 37–53 (2016).
41. Krämer, A., Green, J., Pollard, J. & Tugendreich, S. Causal analysis approaches in ingenuity pathway analysis. *Bioinformatics* **30**, 523–530 (2014).
42. Tong, B. C. K., Wu, A. J., Li, M. & Cheung, K. H. Calcium signaling in Alzheimer's disease & therapies. *Biochim. Biophys. Acta Mol. Cell Res.* **1865**, 1745–1760 (2018).
43. Hampel, H. et al. Measurement of phosphorylated tau epitopes in the differential diagnosis of Alzheimer disease: a comparative cerebrospinal fluid study. *Arch. Gen. Psychiatry* **61**, 95–102 (2004).
44. Suárez-Calvet, M. et al. Novel tau biomarkers phosphorylated at T181, T217 or T231 rise in the initial stages of the preclinical Alzheimer's continuum when only subtle changes in Aβ pathology are detected. *EMBO Mol. Med.* https://doi.org/10.15252/emmm.202012921 (2020).
45. Chen, J. et al. Netrin-1 prevents rat primary cortical neurons from apoptosis via the DCC/ERK pathway. *Front. Cell. Neurosci*. https://doi.org/10.3389/fncel.2017.00387 (2017).
46. Gu, C. et al. ZNRF2 attenuates focal cerebral ischemia/reperfusion injury in rats by inhibiting mTORC1-mediated autophagy. *Exp. Neurol*. https://doi.org/10.1016/j.expneurol.2021.113759 (2021).
47. Lim, S. et al. Amyloid-β precursor protein promotes cell proliferation and motility of advanced breast cancer. *BMC Cancer* https://doi.org/10.1186/1471-2407-14-928 (2014).
48. Grubman, A. et al. A single-cell atlas of entorhinal cortex from individuals with Alzheimer's disease reveals cell-type-specific gene expression regulation. *Nat. Neurosci.* **22**, 2087–2097 (2019).
49. van Hengel, J. et al. Mutations in the area composita protein αT-catenin are associated with arrhythmogenic right ventricular cardiomyopathy. *Eur. Heart J.* **34**, 201–210 (2013).
50. Miller, J. P., Moldenhauer, H. J., Keros, S. & Meredith, A. L. An emerging spectrum of variants and clinical features in KCNMA1-linked channelopathy. *Channels* **15**, 447–464 (2021).
51. Rask-Andersen, M., Masuram, S. & Schiöth, H. B. The druggable genome: evaluation of drug targets in clinical trials suggests major shifts in molecular class and indication. *Annu. Rev. Pharmacol. Toxicol.* **54**, 9–26 (2014).
52. Hori, Y. et al. FDA approved asthma therapeutic agent impacts amyloid β in the brain in a transgenic model of Alzheimer's disease. *J. Biol. Chem*. https://doi.org/10.1074/jbc.M114.586602 (2014).
53. Klein, C. Genetics in dystonia. *Parkinsonism Relat. Disord*. https://doi.org/10.1016/S1353-8020(13)70033-6 (2014).
54. Alzheimer's Association Calcium Hypothesis Workgroup. Calcium hypothesis of Alzheimer's disease and brain aging: a framework for integrating new evidence into a comprehensive theory of pathogenesis. *Alzheimers. Dement*. https://doi.org/10.1016/j.jalz.2016.12.006 (2017).
55. Klunk, W. E. et al. Imaging brain amyloid in Alzheimer's disease with Pittsburgh compound-B. *Ann. Neurol.* **55**, 306–319 (2004).
56. Nordberg, A. PET imaging of amyloid in Alzheimer's disease. *Lancet Neurology* **3**, 519–527 (2004).
57. Jagust, W. J. et al. The Alzheimer's disease neuroimaging initiative positron emission tomography core. *Alzheimers Dement.* **6**, 221–229 (2010).
58. Swaminathan, S. et al. Amyloid pathway-based candidate gene analysis of [^{11C}] PiB-PET in the Alzheimer's disease neuroimaging initiative (ADNI) cohort. *Brain Imaging Behav.* **6**, 1–15 (2012).
59. Saykin, A. J. et al. Genetic studies of quantitative MCI and AD phenotypes in ADNI: progress, opportunities, and plans. *Alzheimers Dement.* **11**, 792–814 (2015).
60. Iwatsubo, T. et al. Japanese and North American Alzheimer's disease neuroimaging initiative studies: harmonization for international trials. *Alzheimers Dement.* **14**, 1077–1087 (2018).
61. De Strooper, B. & Karran, E. The cellular phase of Alzheimer's disease. *Cell* **164**, 603–615 (2016).
62. Mathys, H. et al. Single-cell transcriptomic analysis of Alzheimer's disease. *Nature* **570**, 332–337 (2019).
63. Bryois, J. et al. Genetic identification of cell types underlying brain complex traits yields insights into the etiology of Parkinson's disease. *Nat. Genet.* **52**, 482–493 (2020).

64. Kreisl., W. C. et al. PET imaging of neuroinflammation in neurological disorders. *Lancet. Neurol.* **19**, 940–950 (2020).
65. Newcombe, E. A. et al. Inflammation: the link between comorbidities, genetics, and Alzheimer's disease. *J. Neuroinflammation* https://doi.org/10.1186/s12974-018-1313-3 (2018).
66. Onyango, I. G., Jauregui, G. V., Čarna, M., Bennett, J. P. Jr & Stokin, G. B. Neuroinflammation in Alzheimer's disease. *Biomedicines* https://doi.org/10.3390/biomedicines9050524 (2021).
67. Arboleda-Velasquez, J. F. et al. Resistance to autosomal dominant Alzheimer's disease in an APOE3 Christchurch homozygote: a case report. *Nat. Med.* **25**, 1680–1683 (2019).
68. Alqudah, A. M., Sallam, A., Baenziger, P. S. & Börner, A. GWAS: fast-forwarding gene identification and characterization in temperate cereals: lessons from barley—a review. *J. Adv. Res.* **22**, 119–135 (2019).
69. Blennow, K. et al. Predicting clinical decline and conversion to Alzheimer's disease or dementia using novel Elecsys Aβ(1–42), pTau and tTau CSF immunoassays. *Sci. Rep.* **9**, 1–11 (2019).
70. Van der Auwera, G. A. et al. From fastQ data to high-confidence variant calls: the genome analysis toolkit best practices pipeline. *Curr. Protoc. Bioinformatics* https://doi.org/10.1002/0471250953.bi1110s43 (2013).

Acknowledgements

We express sincere gratitude to all our co-workers and collaborators; to H. Kobayashi, W. Shin and A. Nabetani for experimental support and intellectual debt; to T. Enami and I. Inoue for technical assistance; and to M. Iijima, M. Yasui, N. Kawabata, T. Saigo, T. Urai and M. Nagata for their valuable administrative support. This research was funded in part by a grant for Core Center for iPS Cell Research of Research Center Network for Realization of Regenerative Medicine from AMED to H.I., Uehara Memorial Foundation to H.I., KAKENHI (21H02807) to H.I., KAKENHI (17K16121) and (20K16599) to T.K., KAKENHI (18K18452) to Y.Y., T.K. and H.I., the invited Project at iACT, Kyoto University Hospital to H.I., Suzuken Memorial Foundation to H.I. and AMED (JP20dk0207045) to T.I. The GTEx Project was supported by the Common Fund of the Office of the Director of the National Institutes of Health (NIH) and by the National Cancer Institute, National Human Genome Research Institute, National Heart, Lung, and Blood Institute, National Institute on Drug Abuse, National Institute of Mental Health and National Institute of Neurological Disorders and Stroke. The data used for the analyses described in this manuscript were obtained from the GTEx portal on 6th July 2021. Data collection and sharing for this project was funded by the ADNI (NIH grant U01 AG024904) and Department of Defense ADNI (award no. W81XWH-12-2-0012). ADNI is funded by the National Institute on Aging, the National Institute of Biomedical Imaging and Bioengineering and through contributions from the following: Alzheimer's Association; Alzheimer's Drug Discovery Foundation; Araclon Biotech; BioClinica; Biogen Idec; Bristol-Myers Squibb Company; Eisai; Elan Pharmaceuticals; Eli Lilly and Company; EuroImmun; F. Hoffmann-La Roche and its affiliated company Genentech; Fujirebio; GE Healthcare; IXICO; Janssen Alzheimer Immunotherapy Research & Development; Johnson & Johnson Pharmaceutical Research & Development; Medpace; Merck & Co.; Meso Scale Diagnostics; NeuroRx Research; Neurotrack Technologies; Novartis Pharmaceuticals Corporation; Pfizer; Piramal Imaging; Servier; Synarc and Takeda Pharmaceutical Company. The Canadian Institutes of Health Research is providing funds to support ADNI clinical sites in Canada. Private sector contributions are facilitated by the Foundation for the NIH (www.fnih.org). The grantee organization is the Northern Alzheimer's Disease Cooperative Study at the University of California, San Diego. ADNI data are disseminated by the Laboratory for Neuro Imaging at the University of Southern California. Data used in preparation of this article were obtained from the ADNI database (adni.loni.usc.edu). As such, investigators within ADNI contributed to the design and implementation of ADNI and/or provided data but did not participate in the analysis or writing of this report. A complete listing of ADNI investigators can be found at http://adni.loni.usc.edu/wp-content/uploads/how_to_apply/ADNI_Acknowledgement_List.pdf. The full membership of the J-ADNI investigators is listed at https://humandbs.biosciencedbc.jp/en/hum0043-j-adni-authors.

Author contributions

H.I. conceived the project. T.K. and H.I. designed the experiment. T.K., K.T. and A.N. established iPSCs and iN-iPSCs. T.K. and K.T conducted SNP array analysis. T.K., S.K., Y.Y. and R.Y. conducted CDiP. N.H. and T.I. analyzed the exome database. K.I. analyzed the amyloid PET data. Y.Y. established a prediction algorithm. T. Asada and T. Arai recruited patients.

Competing interests

The authors declare no competing interests.

Additional information

Supplementary information The online version contains supplementary material available at https://doi.org/10.1038/s43587-021-00158-9.

Correspondence and requests for materials should be addressed to Haruhisa Inoue.

Peer review information *Nature Aging* thanks the anonymous reviewers for their contribution to the peer review of this work.

Reprints and permissions information is available at www.nature.com/reprints.

Publisher's note Springer Nature remains neutral with regard to jurisdictional claims in published maps and institutional affiliations.

© The Author(s), under exclusive licence to Springer Nature America, Inc. 2022

Alzheimer's Disease Neuroimaging Initiative (ADNI)

Michael W. Weiner[9], Paul Aisen[10], Ronald Petersen[11], Clifford R. Jack[12], William Jagust[13], John Q. Trojanowki[14], Arthur W. Toga[15], Laurel Beckett[16], Robert C. Green[17], John Morris[18], Leslie M. Shaw[18], Jeffrey Kaye[19], Joseph Quinn[19], Lisa Silbert[19], Betty Lind[19], Raina Carter[19], Sara Dolen[19], Lon S. Schneider[15], Sonia Pawluczyk[15], Mauricio Beccera[15], Liberty Teodoro[15], Bryan M. Spann[15], James Brewer[20], Helen Vanderswag[20], Adam Fleisher[20], Judith L. Heidebrink[21], Joanne L. Lord[21], Sara S. Mason[9], Colleen S. Albers[9], David Knopman[9], Kris Johnson[9], Rachelle S. Doody[22], Javier Villanueva-Meyer[22], Munir Chowdhury[22], Susan Rountree[22], Mimi Dang[22], Yaakov Stern[23], Lawrence S. Honig[23], Karen L. Bell[23], Beau Ances[18], John C. Morris[18], Maria Carroll[18], Mary L. Creech[18], Erin Franklin[18], Mark A. Mintun[18], Stacy Schneider[18], Angela Oliver[18], Daniel Marson[24], Randall Griffith[24], David Clark[24], David Geldmacher[24], John Brockington[24], Erik Roberson[24], Marissa Natelson Love[24], Hillel Grossman[25], Effie Mitsis[25], Raj C. Shah[26], Leyla deToledo-Morrell[26], Ranjan Duara[27], Daniel Varon[27], Maria T. Greig[27], Peggy Roberts[27], Marilyn Albert[28], Chiadi Onyike[28], Daniel D'Agostino[28], Stephanie Kielb[28], James E. Galvin[29], Brittany Cerbone[29], Christina A. Michel[29], Dana M. Pogorelec[29], Henry Rusinek[29], Mony J. de Leon[29], Lidia Glodzik[29], Susan De Santi[29], P. Murali Doraiswamy[30], Jeffrey R. Petrella[30], Salvador Borges-Neto[30], Terence Z. Wong[30], Edward Coleman[30], Charles D. Smith[31], Greg Jicha[31], Peter Hardy[31], Partha Sinha[31], Elizabeth Oates[31], Gary Conrad[31], Anton P. Porsteinsson[32],

Bonnie S. Goldstein[32], Kim Martin[32], Kelly M. Makino[32], M. Saleem Ismail[32], Connie Brand[32], Ruth A. Mulnard[33], Gaby Thai[33], Catherine Mc-Adams-Ortiz[33], Kyle Womack[34], Dana Mathews[34], Mary Quiceno[34], Allan I. Levey[35], James J. Lah[35], Janet S. Cellar[35], Jeffrey M. Burns[36], Russell H. Swerdlow[36], William M. Brooks[36], Liana Apostolova[37], Kathleen Tingus[38], Ellen Woo[38], Daniel H. S. Silverman[38], Po H. Lu[38], George Bartzokis[38], Neill R. Graff-Radford[39], Francine Parfitt[39], Tracy Kendall[39], Heather Johnson[39], Martin R. Farlow[37], Ann Marie Hake[37], Brandy R. Matthews[37], Jared R. Brosch[37], Scott Herring[37], Cynthia Hunt[37], Christopher H. van Dyck[40], Richard E. Carson[40], Martha G. MacAvoy[40], Pradeep Varma[40], Howard Chertkow[41], Howard Bergman[41], Chris Hosein[41], Sandra Black[42], Bojana Stefanovic[42], Curtis Caldwell[42], Ging-Yuek Robin Hsiung[43], Howard Feldman[43], Benita Mudge[43], Michele Assaly[43], Elizabeth Finger[44], Stephen Pasternack[44], Irina Rachisky[44], Dick Trost[44], Andrew Kertesz[44], Charles Bernick[45], Donna Munic[45], Marek Marsel Mesulam[46], Kristine Lipowski[46], Sandra Weintraub[46], Borna Bonakdarpour[46], Diana Kerwin[46], Chuang-Kuo Wu[46], Nancy Johnson[46], Carl Sadowsky[47], Teresa Villena[47], Raymond Scott Turner[48], Kathleen Johnson[48], Brigid Reynolds[48], Reisa A. Sperling[49], Keith A. Johnson[49], Gad Marshall[49], Jerome Yesavage[50], Joy L. Taylor[50], Barton Lane[50], Allyson Rosen[50], Jared Tinklenberg[50], Marwan N. Sabbagh[51], Christine M. Belden[51], Sandra A. Jacobson[51], Sherye A. Sirrel[51], Neil Kowall[52], Ronald Killiany[52], Andrew E. Budson[52], Alexander Norbash[52], Patricia Lynn Johnson[52], Thomas O. Obisesan[53], Saba Wolday[53], Joanne Allard[53], Alan Lerner[54], Paula Ogrocki[54], Curtis Tatsuoka[54], Parianne Fatica[54], Evan Fletcher[55], Pauline Maillard[55], John Olichney[55], Charles DeCarli[55], Owen Carmichael[55], Smita Kittur[56], Michael Borrie[57], T.-Y. Lee[57], Rob Bartha[57], Sterling Johnson[58], Sanjay Asthana[58], Cynthia M. Carlsson[58], Steven G. Potkin[59], Adrian Preda[59], Dana Nguyen[59], Pierre Tariot[60], Anna Burke[60], Nadira Trncic[60], Adam Fleisher[60], Stephanie Reeder[60], Vernice Bates[61], Horacio Capote[61], Michelle Rainka[61], Douglas W. Scharre[62], Maria Kataki[62], Anahita Adeli[62], Earl A. Zimmerman[63], Dzintra Celmins[63], Alice D. Brown[63], Godfrey D. Pearlson[64], Karen Blank[64], Karen Anderson[64], Laura A. Flashman[65], Marc Seltzer[65], Mary L. Hynes[65], Robert B. Santulli[65], Kaycee M. Sink[66], Leslie Gordineer[66], Jeff D. Williamson[66], Pradeep Garg[66], Franklin Watkins[66], Brian R. Ott[67], Henry Querfurth[67], Geoffrey Tremont[67], Stephen Salloway[68], Paul Malloy[68], Stephen Correia[68], Howard J. Rosen[69], Bruce L. Miller[69], David Perry[69], Jacobo Mintzer[70], Kenneth Spicer[70], David Bachman[70], Nunzio Pomara[71], Raymundo Hernando[71], Antero Sarrael[71], Norman Relkin[72], Gloria Chaing[72], Michael Lin[72], Lisa Ravdin[72], Amanda Smith[73], Balebail Ashok Raj[73] and Kristin Fargher[73]

[9]Magnetic Resonance Unit at the VA Medical Center and Radiology, Medicine, Psychiatry and Neurology, University of California, San Francisco, CA, USA. [10]UC San Diego School of Medicine, University of California, La Jolla, CA, USA. [11]Neurology, Mayo Clinic, Rochester, MN, USA. [12]Radiology, Mayo Clinic, Rochester, MN, USA. [13]University of California, Berkeley, Berkeley, CA, USA. [14]University of Pennsylvania, Philadelphia, PA, USA. [15]University of Southern California, Los Angeles, CA, USA. [16]University of California, Davis, Davis, CA, USA. [17]Brigham and Women's Hospital and Harvard Medical School, Boston, MA, USA. [18]Washington University, St. Louis, MO, USA. [19]Oregon Health and Science University, Portland, OR, USA. [20]University of California, San Diego, San Diego, CA, USA. [21]University of Michigan, Ann Arbor, MI, USA. [22]Baylor College of Medicine, Houston, TX, USA. [23]Columbia University Medical Center, New York, NY, USA. [24]University of Alabama, Birmingham, AL, USA. [25]Mount Sinai School of Medicine, New York, NY, USA. [26]Rush University Medical Center, Chicago, IL, USA. [27]Wien Center, Miami Beach, FL, USA. [28]Johns Hopkins University, Baltimore, MD, USA. [29]New York University, New York, NY, USA. [30]Duke University Medical Center, Durham, NC, USA. [31]University of Kentucky, Lexington, KY, USA. [32]University of Rochester Medical Center, Rochester, NY, USA. [33]University of California, Irvine, Irvine, CA, USA. [34]University of Texas Southwestern Medical School, Dallas, TX, USA. [35]Emory University, Atlanta, GA, USA. [36]University of Kansas Medical Center, Kansas City, KS, USA. [37]Indiana University, Bloomington, IN, USA. [38]Universityof California, Los Angeles, Los Angeles, CA, USA. [39]Mayo Clinic, Jacksonville, FL, USA. [40]Yale University School of Medicine, New Haven, CT, USA. [41]McGill University and Jewish General Hospital, Montreal, Quebec, Canada. [42]Sunnybrook Health Sciences Centre, Toronto, Ontario, Canada. [43]UBC Clinic for Alzheimer Disease and Related Disorders, Vancouver, British Columbia, Canada. [44]Cognitive Neurology–St. Joseph's, London, Ontario, Canada. [45]Cleveland Clinic Lou Ruvo Center for Brain Health, Las Vegas, NV, USA. [46]Northwestern University, Evanston, IL, USA. [47]Premiere Research Institute and Palm Beach Neurology, West Palm Beach, FL, USA. [48]Georgetown University Medical Center, Washington, DC, USA. [49]Brigham and Women's Hospital, Boston, MA, USA. [50]Stanford University, Stanford, CA, USA. [51]Banner Sun Health Research Institute, Sun City, AZ, USA. [52]Boston University, Boston, MA, USA. [53]Howard University, Boston, DC, USA. [54]Case Western Reserve University, Cleveland, OH, USA. [55]UC Davis School of Medicine, Sacramento, CA, USA.

[56]Neurological Care of CNY, Syracuse, NY, USA. [57]Parkwood Hospital, Philadelphia, PA, USA. [58]University of Wisconsin, Madison, WI, USA. [59]University of California, Irvine, Irvine, CA, USA. [60]Banner Alzheimer's Institute, Phoenix, AZ, USA. [61]DENT Neurologic Institute, New York, NY, USA. [62]Ohio State University, Columbus, OH, USA. [63]Albany Medical College, Albany, NY, USA. [64]Hartford Hospital, Olin Neuropsychiatry Research Center, Hartford, CT, USA. [65]Dartmouth-Hitchcock Medical Center, Lebanon, NH, USA. [66]Wake Forest University Health Sciences, Winston-Salem, NC, USA. [67]Rhode Island Hospital, Providence, RI, USA. [68]Butler Hospital, Providence, RI, USA. [69]University of California, San Francisco, San Francisco, CA, USA. [70]Medical University of South Carolina, Charleston, SC, USA. [71]Nathan Kline Institute, Orangeburg, NY, USA. [72]Cornell University, Ithaca, NY, USA. [73]USF Health Byrd Alzheimer's Institute, University of South Florida, Tampa, FL, USA.

Japanese Alzheimer's Disease Neuroimaging Initiative (J-ADNI)

Takeshi Iwatsubo[74], Takashi Asada[75], Hiroyuki Arai[76], Morihiro Sugishita[77], Hiroshi Matsuda[78], Kengo Ito[79], Michio Senda[80], Kenji Ishii[81], Ryozo Kuwano[82], Takeshi Ikeuchi[82], Noriko Sato[78], Hajime Sato[78], Shun Shimohama[83], Masaki Saitoh[83], Rika Yamauchi[83], Takashi Hayashi[83], Seiju Kobayashi[84], Norihito Nakano[85], Junichiro Kanazawa[86], Takeshi Ando[87], Chiyoko Takanami[83], Masato Hareyama[88], Masamitsu Hatakenaka[89], Eriko Tsukamoto[90], Shinji Ochi[91], Mikio Shoji[92], Etsuro Matsubara[92], Takeshi Kawarabayashi[92], Yasuhito Wakasaya[92], Takashi Nakata[92], Naoko Nakahata[92], Shuichi Ono[93], Yoshihiro Takai[93], Satoshi Takahashi[94], Hisashi Yonezawa[94], Junko Takahashi[94], Masako Kudoh[94], Makoto Sasaki[95], Yutaka Matsumura[96], Yohsuke Hirata[96], Tsuyoshi Metoki[96], Susumu Hayakawa[96], Yuichi Sato[96], Masayuki Takeda[96], Toshiaki Sasaki[97], Koichiro Sera[96], Kazunori Terasaki[96], Yoshihiro Saitoh[98], Shoko Goto[98], Kuniko Ueno[94], Hiromi Sakashita[94], Kuniko Watanabe[94], Ken Nagata[99], Yuichi Sato[99], Tetsuya Maeda[99], Yasushi Kondoh[99], Takashi Yamazaki[99], Daiki Takano[99], Mio Miyata[99], Hiromi Komatsu[99], Mayumi Watanabe[99], Tomomi Sinoda[99], Rena Muraoka[99], Kayoko Kikuchi[100], Hitomi Ito[101], Aki Sato[101], Toshibumi Kinoshita[102], Hideyo Toyoshima[102], Kaoru Sato[102], Shigeki Sugawara[102], Isao Ito[103], Fumiko Kumagai[103], Hiroyuki Arai[104], Katsutoshi Furukawa[104], Masaaki Waragai[104], Naoki Tomita[104], Nobuyuki Okamura[105], Mari Ootsuki[104], Katsumi Sugawara[104], Satomi Sugawara[104], Shunji Mugikura[106], Atsushi Umetsu[106], Takanori Murata[106], Tatsuo Nagasaka[106], Yukitsuka Kudo[107], Manabu Tashiro[108], Shoichi Watanuki[108], Masatoyo Nishizawa[109], Takeshi Ikeuchi[109], Takayoshi Tokutake[109], Saeri Ishikawa[110], Emiko Kishida[110], Nozomi Sato[110], Mieko Hagiwara[111], Kumi Yamanaka[111], Takeyuki Watanabe[111], Taeko Takasugi[111], Shoichi Inagawa[112], Kenichi Naito[112], Masanori Awaji[112], Tsutomu Kanazawa[112], Kouiti Okamoto[113], Masaki Ikeda[113], Tsuneo Yamazaki[114], Yuiti Tasiro[113], Syunn Nagamine[113], Shiori Katsuyama[114], Sathiko Kurose[113], Sayuri Fukushima[115], Etsuko Koya[115], Makoto Amanuma[116], Noboru Oriuti[117], Kouiti Ujita[116], Kazuhiro Kishi[116], Kazuhisa Tuda[116], Takashi Asada[118], Katsuyoshi Mizukami[118], Tetsuaki Arai[118], Etsuko Nakajima[118], Katsumi Miyamoto[119], Kousaku Saotome[120], Tomoya Kobayashi[119], Saori Itoya[119], Jun Ookubo[119], Toshiya Akatsu[119], Yoshiko Anzai[119], Junya Ikegaki[119], Yuuichi Katou[119], Kaori Kimura[119], Ryou Kuchii[120], Hajime Saitou[119], Kazuya Shinoda[119], Satoka Someya[119], Hiroko Taguchi[119], Kazuya Tashiro[119], Masaya Tanaka[119], Tatsuya Nemoto[119], Ryou Wakabayashi[119], Daisuke Watanabe[119], Harumasa Takano[121], Tetsuya Suhara[121], Hitoshi Shinoto[121], Hitoshi Shimada[121], Makoto Higuchi[121], Takaaki Mori[121], Hiroshi Ito[122], Takayuki Obata[122], Yoshiko Fukushima[123], Kazuko Suzuki[123], Izumi Izumida[123], Katsuyuki Tanimoto[124], Takahiro Shiraishi[124], Hitoshi Shinotoh[125], Hitoshi Shimada[125], Junko Shiba[125], Hiroaki Yano[125], Miki Satake[125], Aimi Nakui[125], Yae Ebihara[125], Tomomi Hasegawa[125], Yasumasa Yoshiyama[126], Mami Kato[126], Yuki Ogata[126], Hiroyuki Fujikawa[126], Nobuo Araki[127], Yoshihiko Nakazato[127], Takahiro Sasaki[127], Tomokazu Shimadu[127], Kimiko Yoshimaru[127], Hiroshi Matsuda[128], Etsuko Imabayashi[128], Asako Yasuda[128], Etuko Yamamoto[129], Natsumi Nakamata[129], Noriko Miyauchi[129], Keiko Ozawa[128], Rieko Hashimoto[130], Taishi Unezawa[130],

Takafumi Ichikawa[130], Hiroki Hayashi[130], Masakazu Yamagishi[130], Tunemichi Mihara[130], Masaya Hirano[130], Shinichi Watanabe[130], Junichiro Fukuhara[131], Hajime Matsudo[131], Nobuyuki Saito[132], Atsushi Iwata[133], Hisatomo Kowa[133], Toshihiro Hayashi[133], Ryoko Ihara[133], Toji Miyagawa[133], Mizuho Yoshida[133], Yuri Koide[133], Eriko Samura[133], Kurumi Fujii[133], Kaori Watanabe[134], Nagae Orihara[134], Toshimitsu Momose[135], Akira Kunimatsu[136], Harushi Mori[136], Miwako Takahashi[135], Takuya Arai[135], Yoshiki Kojima[135], Masami Goto[137], Takeo Sarashina[137], Syuichi Uzuki[137], Seiji Katou[137], Yoshiharu Sekine[137], Yukihiro Takauchi[137], Chiine Kagami[138], Kazutomi Kanemaru[139], Shigeo Murayama[140], Yasushi Nishina[139], Kenji Ishii[140], Maria Sakaibara[139], Yumiko Okazaki[139], Rieko Okada[139], Maki Obata[139], Yuko Iwata[141], Mizuho Minami[141], Yasuko Hanabusa[141], Hanae Shingyouji[141], Kyoko Tottori[141], Aya Tokumaru[142], Makoto Ichinose[142], Kazuya Kume[142], Syunsuke Kahashi[142], Kunimasa Arima[143], Tadashi Tukamoto[144], Shin Tanaka[143], Yuko Nagahusa[143], Masuhiro Sakata[143], Mitsutoshi Okazaki[143], Yuko Saito[143], Maki Yamada[143], Tiine Kodama[145], Maki Obata[145], Tomoko Takeuchi[145], Keiichiro Ozawa[145], Yuko Iwata[146], Hanae Shingyouji[146], Yasuko Hanabusa[146], Yoshiko Kawaji[146], Kyouko Tottori[146], Noriko Sato[147], Yasuhiro Nakata[147], Satoshi Sawada[147], Makoto Mimatsu[147], Daisuke Nakkamura[147], Takeshi Tamaru[147], Shunichirou Horiuchi[147], Heii Arai[148], Tsuneyoshi Ota[148], Aiko Kodaka[148], Yuko Tagata[148], Tomoko Nakada[148], Eizo Iseki[149], Kiyoshi Sato[149], Hiroshige Fujishiro[150], Norio Murayama[151], Masaru Suzuki[152], Satoshi Kimura[152], Masanobu Takahashi[152], Haruo Hanyu[153], Hirofumi Sakurai[153], Takahiko Umahara[153], Hidekazu Kanetaka[153], Kaori Arashino[153], Mikako Murakami[153], Ai Kito[153], Seiko Miyagi[154], Kaori Doi[154], Kazuyoshi Sasaki[154], Mineo Yamazaki[155], Akiko Ishiwata[155], Yasushi Arai[155], Akane Nogami[155], Sumiko Fukuda[155], Kyouko Tottori[156], Mizuho Minami[156], Yuko Iwata[156], Koichi Kozaki[157], Yukiko Yamada[157], Sayaka Kimura[157], Ayako Machida[157], Kuninori Kobayashi[158], Hidehiro Mizusawa[159], Nobuo Sanjo[159], Mutsufusa Watanabe[159], Takuya Ohkubo[159], Hiromi Utashiro[159], Yukiko Matsumoto[159], Kumiko Hagiya[159], Yoshiko Miyama[159], Takako Shinozaki[160], Haruko Hiraki[160], Hitoshi Shibuya[159], Isamu Ohashi[159], Akira Toriihara[159], Shinichi Ohtani[161], Toshifumi Matsui[162], Yu Hayasaka[163], Tomomi Toyama[162], Hideki Sakurai[162], Kumiko Sugiura[162], Hirofumi Taguchi[164], Shizuo Hatashita[165], Akari Imuta[166], Akiko Matsudo[166], Daichi Wakebe[167], Hideki Hayakawa[167], Mitsuhiro Ono[167], Takayoshi Ohara[167], Yukihiko Washimi[168], Yutaka Arahata[168], Akinori Takeda[168], Yoko Konagaya[169], Akiko Yamaoka[168], Masashi Tsujimoto[168], Hideyuki Hattori[170], Takashi Sakurai[171], Miura Hisayuki[172], Hidetoshi Endou[173], Syousuke Satake[174], Young Jae Hong[174], Katsunari Iwai[175], Kenji Yoshiyama[170], Masaki Suenaga[175], Sumiko Morita[175], Teruhiko Kachi[79], Kenji Toba[79], Rina Miura[170], Takiko Kawai[168], Ai Honda[168], Kengo Itou[176], Takashi Kato[176], Ken Fujiwara[176], Rikio Katou[177], Mariko Koyama[177], Naohiko Fukaya[177], Akira Tsuji[177], Hitomi Shimizu[177], Hiroyuki Fujisawa[177], Tomoko Nakazawa[177], Satoshi Koyama[177], Takanori Sakata[177], Masahito Yamada[178], Mitsuhiro Yoshita[178], Miharu Samuraki[178], Kenjiro Ono[178], Moeko Shinohara[178], Yuki Soshi[178], Kozue Niwa[178], Chiaki Doumoto[178], Mariko Hata[179], Miyuki Matsushita[179], Mai Tsukiyama[179], Nozomi Takeda[180], Sachiko Yonezawa[180], Ichiro Matsunari[180], Osamu Matsui[181], Fumiaki Ueda[181], Yasuji Ryu[181], Masanobu Sakamoto[182], Yasuomi Ouchi[182], Yasuomi Ouchi[183], Madoka Chita[184], Yumiko Fujita[182], Rika Majima[185], Hiromi Tsubota[186], Umeo Shirasawa[187], Masashi Sugimori[187], Wataru Ariya[187], Yuuzou Hagiwara[187], Yasuo Tanizaki[187], Hidenao Fukuyama[188], Ryosuke Takahashi[189], Hajime Takechi[190], Chihiro Namiki[191], Kengo Uemura[189], Takeshi Kihara[192], Hiroshi Yamauchi[193], Shizuko Tanaka-Urayama[188], Emiko Maeda[194], Natsu Saito[195], Shiho Satomi[196], Konomi Kabata[197], Shin-Ichi Urayama[188], Tomohisa Okada[198], Koichi Ishizu[199], Shigeto Kawase[200],

Satoshi Fukumoto[200], Masanori Nakagawa[201], Takahiko Tokuda[202], Masaki Kondo[201], Fumitoshi Niwa[201], Toshiki Mizuno[201], Yoko Oishi[201], Mariko Yamazaki[201], Daisuke Yamaguchi[201], Kyoko Ito[203], Yoku Asano[203], Chizuru Hamaguchi[203], Kei Yamada[204], Chio Okuyama[204], Kentaro Akazawa[204], Shigenori Matsushima[204], Takamasa Matsuo[205], Toshiaki Nakagawa[205], Takeshi Nii[205], Takuji Nishida[205], Kuniaki Kiuchi[206], Masami Fukusumi[207], Hideyuki Watanabe[208], Toshiaki Taoka[209], Akihiro Nogi[210], Masatoshi Takeda[211], Toshihisa Tanaka[211], Naoyuki Sato[212], Hiroaki Kazui[211], Kenji Yoshiyama[211], Takashi Kudo[211], Masayasu Okochi[211], Takashi Morihara[211], Shinji Tagami[211], Noriyuki Hayashi[213], Masahiko Takaya[211], Tamiki Wada[211], Mikiko Yokokoji[211], Hiromichi Sugiyama[211], Daisuke Yamamoto[211], Shuko Takeda[214], Keiko Nomura[211], Mutsumi Tomioka[211], Eiichi Uchida[215], Yoshiyuki Ikeda[215], Mineto Murakami[215], Takami Miki[216], Hiroyuki Shimada[216], Suzuka Ataka[216], Motokatsu Kanemoto[217], Jun Takeuchi[218], Akitoshi Takeda[216], Rie Azuma[219], Yuki Iwamoto[216], Naomi Tagawa[220], Junko Masao[220], Yuka Matsumoto[220], Yuko Kikukawa[220], Hisako Fujii[220], Junko Matsumura[220], Susumu Shiomi[221], Joji Kawabe[221], Yoshihiro Shimonishi[222], Yukio Miki[223], Mitsuji Higashida[222], Tomohiro Sahara[222], Takashi Yamanaga[222], Shinichi Sakamoto[223], Hiroyuki Tsushima[224], Kiyoshi Maeda[225], Yasuji Yamamoto[225], Toshio Kawamata[226], Kazuo Sakai[225], Haruhiko Oda[225], Takashi Sakurai[227], Taichi Akisaki[227], Mizuho Adachi[228], Masako Kuranaga[228], Sachi Takegawa[228], Yoshihiko Tahara[225], Seishi Terada[229], Takeshi Ishihara[230], Hajime Honda[231], Osamu Yokota[231], Yuki Kishimoto[229], Naoya Takeda[229], Nao Imai[229], Mayumi Yabe[229], Kentaro Ida[232], Daigo Anami[233], Seiji Inoue[233], Toshi Matsushita[233], Reiko Wada[229], Shinsuke Hiramatsu[234], Hiromi Tonbara[235], Reiko Yamamoto[235], Kenji Nakashima[236], Kenji Wada-Isoe[236], Saori Yamasaki[236], Eijiro Yamashita[237], Yu Nakamura[238], Ichiro Ishikawa[238], Sonoko Danjo[238], Tomomi Shinohara[238], Miyuki Ueno[239], Yuka Kashimoto[238], Yoshihiro Nishiyama[240], Yuka Yamamoto[240], Narihide Kimura[240], Kazuo Ogawa[241], Yasuhiro Sasakawa[241], Takashi Ishimori[241], Yukito Maeda[241], Tatsuo Yamada[242], Shinji Ouma[242], Aika Fukuhara-Kaneumi[242], Nami Sakamoto[243], Rie Nagao[243], Kengo Yoshimitsu[244], Yasuo Kuwabara[244], Ryuji Nakamuta[245], Minoru Tanaka[245], Manabu Ikeda[246], Mamoru Hashimoto[247], Keiichirou Kaneda[247], Yuusuke Yatabe[246], Kazuki Honda[247], Naoko Ichimi[247], Fumi Akatuka[248], Mariko Morinaga[247], Miyako Noda[247], Mika Kitajima[249], Toshinori Hirai[250], Shinya Shiraishi[250], Naoji Amano[251], Shinsuke Washizuka[251], Toru Takahashi[252], Shin Inuzuka[252], Tetsuya Hagiwara[251], Nobuhiro Sugiyama[252], Yatsuka Okada[251], Tomomi Ogihara[251], Takehiko Yasaki[252], Minori Kitayama[252], Tomonori Owa[252], Akiko Ryokawa[252], Rie Takeuchi[253], Satoe Goto[253], Keiko Yamauchi[253], Mie Ito[253], Tomoki Kaneko[254], Hitoshi Ueda[255], Shuichi Ikeda[256], Masaki Takao[140,257], Ban Mihara[257], Hirofumi Kubo[257], Akiko Takano[257], Gou Yasui[257], Masami Akuzawa[257], Kaori Yamaguchi[257], Toshinari Odawara[258], Megumi Shimamura[259], Mikiko Sugiyama[259], Atsushi Watanabe[260], Naomi Oota[258], Shigeo Takebayashi[261], Yoshigazu Hayakawa[261], Mitsuhiro Idegawa[261], Noriko Toya[261] and Kazunari Ishii[262]

[74]University of Tokyo, Tokyo, Japan. [75]Tsukuba University, Tsukuba, Japan. [76]Tohoku University, Sendai, Japan. [77]Institute of Brain and Blood Vessels, Isesaki, Japan. [78]National Center of Neurology and Psychiatry, Kodaira, Japan. [79]National Center of Geriatrics and Gerontology, Tokyo, Japan. [80]Institute of Biomedical Research and Innovation, Kobe, Japan. [81]Tokyo Metropolitan Geriatric Hospital and Institute of Gerontology, Tokyo, Japan. [82]Niigata University, Niigata, Japan. [83]Department of Neurology, Sapporo Medical University, Sapporo, Japan. [84]Department of Neuropsychiatry, Sapporo Medical University, Sapporo, Japan. [85]Department of Clinical Psychology, School of Psychological Science, Health Sciences University of Hokkaido, Sapporo, Japan. [86]School of Psychological Science, Health Sciences University of Hokkaido, Sapporo, Japan. [87]Graduate School of Psychological Science, Health Sciences University of Hokkaido, Sapporo, Japan. [88]Department of Radiology, Sapporo Medical University, Sapporo, Japan. [89]Division of Diagnostic Radiology, Sapporo Medical University, Sapporo, Japan. [90]Social Medical Corporation Teishinkai Central CI Clinic, Sapporo, Japan. [91]Radiology Department, Social Medical Corporation Teishinkai Central CI Clinic, Sapporo, Japan. [92]Department of Neurology, Hirosaki University Graduate School of Medicine, Hirosaki, Japan. [93]Department of Radiology, Hirosaki University Graduate School of Medicine, Hirosaki, Japan. [94]Division of Neurology and Gerontology, Department of Internal Medicine, Iwate Medical University, Morioka, Japan. [95]Division of Ultrahigh Field MRI, Institute for Biomedical Sciences, Iwate Medical University, Morioka, Japan.

[96]Center for Radiological Sciences, Iwate Medical University, Morioka, Japan. [97]Cyclotron Research Center, Iwate Medical University, Morioka, Japan. [98]Nishina Memorial Cyclotron Center, Japan Radioisotope Association, Takizawa, Japan. [99]Departmetnt of Neurology, Research Institute for Brain and Blood Vessels-Akita, Akita, Japan. [100]Pharmacy, Research Institute for Brain and Blood Vessels-Akita, Akita, Japan. [101]Medical Support Department, Research Institute for Brain and Blood Vessels-Akita, Akita, Japan. [102]Department of Radiology, Research Institute for Brain and Blood Vessels-Akita, Akita, Japan. [103]Clinical Laboratory, Research Institute for Brain and Blood Vessels-Akita, Akita, Japan. [104]Geriatrics and Gerontology, Tohoku University Hospital, Sendai, Japan. [105]Pharamacology, Tohoku University Hospital, Sendai, Japan. [106]RadiologyTohoku University Hospital, Sendai, Japan. [107]Neuroimaging, Tohoku University Hospital, Sendai, Japan. [108]Nuclear Medicine, Tohoku University Hospital, Sendai, Japan. [109]Department of Neurology, Brain Research Institute, Niigata University, Niigata, Japan. [110]Department of Rehabilitation, Niigata University Medical and Dental Hospital, Niigata, Japan. [111]Clinical Research Center, Niigata University Medical and Dental Hospital, Niigata, Japan. [112]Department of Radiology, Niigata University Medical and Dental Hospital, Niigata, Japan. [113]Department of Neurology, Gunma University Hospital, Maebashi, Japan. [114]Department of Health of Rehabilitation, Gunma University Hospital, Maebashi, Japan. [115]Clinical Trial Unit, Gunma University Hospital, Maebashi, Japan. [116]Department of Radiology, Gunma University Hospital, Maebashi, Japan. [117]Department of Nuclear Medicine Image, Gunma University Hospital, Maebashi, Japan. [118]Department of Psychiatry Division of Clinical MedicineFaculty of Medicine, University of Tsukuba, Tsukuba, Japan. [119]Department of Radiological Technology, Tsukuba Medical Center Hospital, Tsukuba, Japan. [120]Former Department of Radiological Technology, Tsukuba Medical Center Hospital, Tsukuba, Japan. [121]Molecular Imaging Center Molecular Neuroimaging Program, National Institute of Radiological Sciences, Chiba, Japan. [122]Molecular Imaging Center Biophysics Program, National Institute of Radiological Sciences, Chiba, Japan. [123]Molecular Imaging Center Planning and Promotion Unit Clinical Research Support Section, National Institute of Radiological Sciences, Chiba, Japan. [124]Hospital Research Center for Charged Particle Therapy Radiological Technology Section, National Institute of Radiological Sciences, Chiba, Japan. [125]Asahi Hospital for Neurological Diseases and Rehabilitation, Matsudo, Japan. [126]National Hospital Organization Chiba East National Hospital, Chiba, Japan. [127]Department of Neurology & Stroke Care Unit, Saitama Medical University Hospital, Moroyama, Japan. [128]Department of Nuclear Medicine, Saitama Medical University Hospital, Moroyama, Japan. [129]Department of Rehabilitation, Saitama Medical University Hospital, Moroyama, Japan. [130]Central Radiology Division, Saitama Medical University Hospital, Moroyama, Japan. [131]Pharmacy Division, Saitama Medical University Hospital, Moroyama, Japan. [132]SHI Accelerator Service Ltd. (SAS), Tokyo, Japan. [133]Department of Neurology, The University of Tokyo Hospital, Tokyo, Japan. [134]Clinical Research Center, The University of Tokyo Hospital, Tokyo, Japan. [135]Department of Nuclear Medicine, The University of Tokyo Hospital, Tokyo, Japan. [136]Department of Diagnostic Radiology, The University of Tokyo Hospital, Tokyo, Japan. [137]Radiological Center, The University of Tokyo Hospital, Tokyo, Japan. [138]Neuroscience, Faculty of Medicine, Graduate School of Medicine, The University of Tokyo, Tokyo, Japan. [139]Department of Neurology, Tokyo Metropolitan Geriatric Hospital, Tokyo, Japan. [140]Tokyo Metropolitan Institute of Gerontology, Tokyo, Japan. [141]Clinical Support Corporation, Tokyo Metropolitan Geriatric Hospital and Institute of Gerontology, Tokyo, Japan. [142]Department of Radiology, Tokyo Metropolitan Geriatric Hospital, Tokyo, Japan. [143]Department of Psychiatry, National Center Hospital National Center of Neurology and Psychiatry, Kodaira, Japan. [144]Department of Neurology, National Center Hospital National Center of Neurology and Psychiatry, Kodaira, Japan. [145]Administration Office of J-ADNI, National Center Hospital National Center of Neurology and Psychiatry, Kodaira, Japan. [146]Clinical Support Corporation, National Center Hospital National Center of Neurology and Psychiatry, Kodaira, Japan. [147]Department of Radiology, National Center Hospital National Center of Neurology and Psychiatry, Tokyo, Japan. [148]Juntendo University Hospital, Mental Clinic, Tokyo, Japan. [149]PET/CT Dementia Research Center, Juntendo Tokyo Koto Geriatric Medical Center, Tokyo, Japan. [150]PET/CT Dementia Research Center, Department of Neuro-Psychiatry, Juntendo Tokyo Koto Geriatric Medical Center, Tokyo, Japan. [151]Department of Neuro-Psychiatry, Juntendo Tokyo Koto Geriatric Medical Center, Tokyo, Japan. [152]Radiology, Juntendo Tokyo Koto Geriatric Medical Center, Tokyo, Japan. [153]Department of Geriatric Medicine, Tokyo Medical University, Tokyo, Japan. [154]Tokyo Medical University, Tokyo, Japan. [155]Division of Neurology, Department of Internal Medicine, Nippon Medical School, Tokyo, Japan. [156]Clinical Support Corporation, Nippon Medical School Hospital, Japan. [157]Geriatric Medicine, Kyorin University, Mitaka, Japan. [158]Radiation Medicine, Kyorin University, Mitaka, Japan. [159]Tokyo Medical and Dental University Graduate school of Medicine and Dental Sciences, Tokyo, Japan. [160]Clinical Research Center, Tokyo Medical and Dental University Hospital Faculty of Medicine, Tokyo, Japan. [161]Department of Radiology, Tokyo Medical and Dental University Hospital Faculty of Medicine, Tokyo, Japan. [162]Clinical Center for Neurodegenerative, National Hospital Organization Kurihama Medical & Addiction Center, Yokosuka, Japan. [163]Department of Psychiatry, Kitasato University School of Medicine, Sagamihara, Japan. [164]Department of Radiology, National Hospital Organization Kurihama Medical & Addiction Center, Yokosuka, Japan. [165]Neurosurgery, Shonan-atsugi Hospital, Atsugi, Japan. [166]Clinical Research Center, Shonan-atsugi Hospital, Atsugi, Japan. [167]Radiology, Shonan-atsugi Hospital, Atsugi, Japan. [168]Department of Cognitive Disorders, National Center of Geriatrics and Gerontology, Obu, Japan. [169]Dementia Care Research and Training Center, National Center of Geriatrics and Gerontology, Obu, Japan. [170]Department of Psychiatry, National Center of Geriatrics and Gerontology, Obu, Japan. [171]Center for Comprehensive Care and Research on Memory Disorders, National Center of Geriatrics and Gerontology, Obu, Japan. [172]Department of Home Medical Care Support, National Center of Geriatrics and Gerontology, Obu, Japan. [173]Department of Comprehensive Geriatric Medicine, National Center of Geriatrics and Gerontology, Obu, Japan. [174]Department of Geriatrics, National Center of Geriatrics and Gerontology, Obu, Japan. [175]Department of Neurology, National Center of Geriatrics and Gerontology, Obu, Japan. [176]Department of Clinical and Experimental Neuroimaging, National Center of Geriatrics and Gerontology, Obu, Japan. [177]Department of Radiology, National Center of Geriatrics and Gerontology, Obu, Japan. [178]Department of Neurology and Neurobiology of Aging, Kanazawa University Graduate School of Medical Science, Kanazawa, Japan. [179]Center for Clinical Research Management, Kanazawa University Hospital, Kanazawa, Japan. [180]The Medical and Pharmacological Research Center Foundation, Kanazawa, Japan. [181]Department of Radiology, Kanazawa University Graduate School of Medical Science, Kanazawa, Japan. [182]Department of Neurology, Hamamatsu Medical Center, Hamamatsu, Japan. [183]Hamamatsu University School of Medicine, Hamamatsu, Japan. [184]Hamamatsu Medical Center, Hamamatsu, Japan. [185]Department of Psychiatry, Hamamatsu Medical Center, Hamamatsu, Japan. [186]Department of Clinical Research Management, Hamamatsu Medical Center, Hamamatsu, Japan. [187]Department of Radiological Technology, Hamamatsu Medical Center, Hamamatsu, Japan. [188]Human Brain Research Center, Kyoto University Graduate School of Medicine, Kyoto, Japan. [189]Department of Neurology, Kyoto University Graduate School of Medicine, Kyoto, Japan. [190]Department of Geriatric Medicine, Kyoto University Graduate School of Medicine, Kyoto, Japan. [191]Eli Lilly Japan K.K Medical Science, Kobe, Japan. [192]Rakuwakai Misasagi Hospital, Kyoto, Japan. [193]Shiga Medical Center Research Institute, Moriyama, Japan. [194]Takemura Clinic, Kyoto, Japan. [195]Tonami General Hospital, Tonami, Japan. [196]University Hospital, Kyoto Prefectural University of Medicine, Kyoto, Japan. [197]Department of Diagnostic Pathology, Kyoto University Hospital, Kyoto, Japan. [198]Department of Diagnostic Imaging and Nuclear Medicine, Kyoto University Graduate School of Medicine, Kyoto, Japan. [199]Department of Human Health Sciences, Kyoto University Graduate School of Medicine, Kyoto, Japan. [200]Department of Radiology and Nuclear Medicine Service, Kyoto University Hospital, Kyoto, Japan. [201]Department of Neurology, Graduate School of Medical Science, Kyoto Prefectural University of Medicine, Kyoto, Japan. [202]Department of Molecular Pathobiology of Brain Diseases (Department of Neurology), Graduate School of Medical Science, Kyoto Prefectural University of Medicine, Kyoto, Japan. [203]Tokyo Yakuriken Co., Ltd, Tokyo, Japan. [204]Department of Radiology, Graduate School of Medical Science, Kyoto Prefectural University of Medicine, Kyoto, Japan. [205]Kyoto Prefectural University of Medicine Hospital, Kyoto, Japan. [206]Department of Psychiatry, Nara Medical University, Kashihara, Japan. [207]Faculty of Psychology, Doshisha University, Kyotanabe, Japan. [208]Heartland Shigisan Hospital, Sango, Japan. [209]Department of Radiology, Nara Medical University, Kashihara, Japan. [210]Central Radiology, Nara Medical University, Kashihara, Japan. [211]Psychiatry, Department of Integrated Medicine, Division of Internal Medicine, Osaka University Graduate School of Medicine, Suita, Japan. [212]Department of Clinical Gene Therapy, Department of Geriatric Medicine, Osaka University Graduate School

of Medicine, Suita, Japan. [213]Department of Complementary and Alternative Medicine, Osaka University Graduate School of Medicine, Suita, Japan. [214]Japan Society for the Promotion of Science, Tokyo, Japan. [215]Uchida Clinic/Department of radiology, Osaka University Graduate School of Medicine, Ibaraki/Suita, Japan. [216]Department of Geriatrics and Neurology, Osaka City University Graduate School of Medicine, Osaka, Japan. [217]Osaka Municipal Kohsaiin Hospital, Suita, Japan. [218]Kishiwada City Hospital, Kishiwada, Japan. [219]Department of Psychiatry, Kosaka Hospital, Higashiosaka, Japan. [220]Osaka City University Hospital Center for Drug and Food Clinical Evaluation, Osaka, Japan. [221]Department of Nuclear Medicine, Osaka City University Graduate School of Medicine, Osaka, Japan. [222]Department of Radiology, Osaka City University Hospital, Osaka, Japan. [223]Department of Radiology, Osaka City University Graduate School of Medicine, Osaka, Japan. [224]Department of Radiological Science, Ibaraki Prefectural University of Health Sciences, Ami, Japan. [225]Department of Psychiatry, Kobe University Graduate School of Medicine, Kobe, Japan. [226]Kobe University Graduate School of Health Sciences, Kobe, Japan. [227]Department of General Internal Medicine, Kobe University Graduate School of Medicine, Kobe, Japan. [228]Derartment of Psychiatry and Neurology, Kobe University Hospital, Kobe, Japan. [229]Department of Psychiatry, Okayama University Graduate School of Medicine, Dentistry and Pharmaceutical, Okayama, Japan. [230]Department of Psychiatry, Kawasaki Hospital, Kurashiki, Japan. [231]Department of Psychiatry, Okayama University Hospital, Okayama, Japan. [232]Department of Imaging Diagnosis, Okayama Diagnostic Imaging Center, Okayama, Okayama, Japan. [233]Department of Imaging Technology, Okayama Diagnostic Imaging Center, Okayama, Okayama, Japan. [234]Department of Administration, Okayama Diagnostic Imaging Center, Okayama, Japan. [235]Okayama University Hospital, Okayama, Japan. [236]Division of Neurology, Department of Brain and Neurosciences, Faculty of Medicine, Tottori University, Yonago, Japan. [237]Division of Clinical Radiology, Tottori University Hospital, Yonago, Japan. [238]Department of Neuropsychiatry Kagawa University School of Medicine, Kagawa, Japan. [239]Kagawa University Hospital Cancer center, Kagawa, Japan. [240]Department of Radiology, Faculty of Medicine, Kagawa University, Kagawa, Japan. [241]Department of Clinical Radiology, Kagawa University Hospital, Kagawa, Japan. [242]Department of Neurology, Fukuoka University, Fukuoka, Japan. [243]Neues Corporation, Tokyo, Japan. [244]Department of Radiology, Fukuoka University, Fukuoka, Japan. [245]Radiology Center, Fukuoka University Hospital, Fukuoka, Japan. [246]Department of Psychiatry and Neuropathobiology, Faculty of Life Science, Kumamoto University, Kumamoto, Japan. [247]Department of Neuropsychiatry, Kumamoto University Hospital, Kumamoto, Japan. [248]A Center of Support for Child Development, Kumamoto University Hospital, Kumamoto, Japan. [249]Department of Medical Imaging, Kumamoto University, Kumamoto, Japan. [250]Department of Diagnostic Imaging, Faculty of Life Science, Kumamoto University, Kumamoto, Japan. [251]Department of Psychiatry, Shinshu University School of Medicine, Matsumoto, Japan. [252]Department of Psychiatry, Shinshu University Hospital, Matsumoto, Japan. [253]Clinical Trial Research Center, Shinshu University Hospital, Matsumoto, Japan. [254]Department of Radiology, Shinshu University School of Medicine, Matsumoto, Japan. [255]Radiology Division, Shinshu University Hospital, Matsumoto, Japan. [256]Department of Medicine (Neurology and Rheumatology), Shinshu University School of Medicine, Matsumoto, Japan. [257]Mihara Memorial Hospital, Isesaki, Japan. [258]Psychiatric Center, Yokohama City University Medical Center, Yokohama, Japan. [259]Neurology, Yokohama City University Medical Center, Yokohama, Japan. [260]Yokohama City University Medical Center, Yokohama, Japan. [261]Radiology, Yokohama City University Medical Center, Yokohama, Japan. [262]Kindai University, Sayama, Japan.

a

	Patients (N = 102)
Gender	34 males, 68 females
Average age at onset (years)	76.0 ± 7.2
Average of ADAS score at biopsy (score)	20.2 ± 6.1
APOE ε4 allele present (%)	58 (56.9%)

b

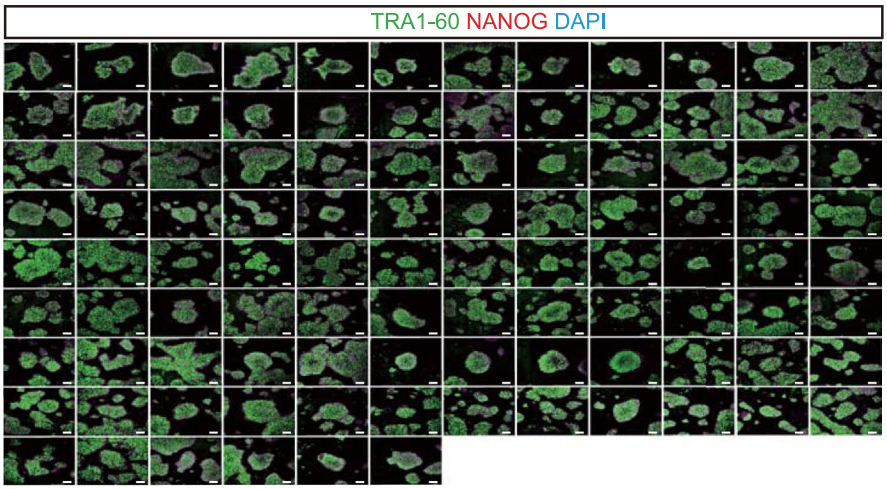

c

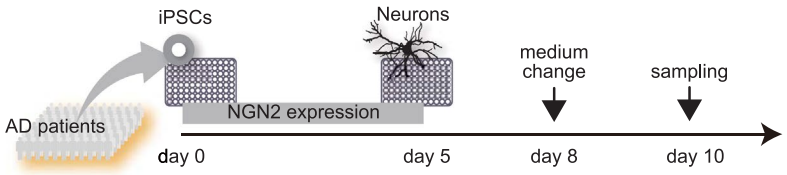

d

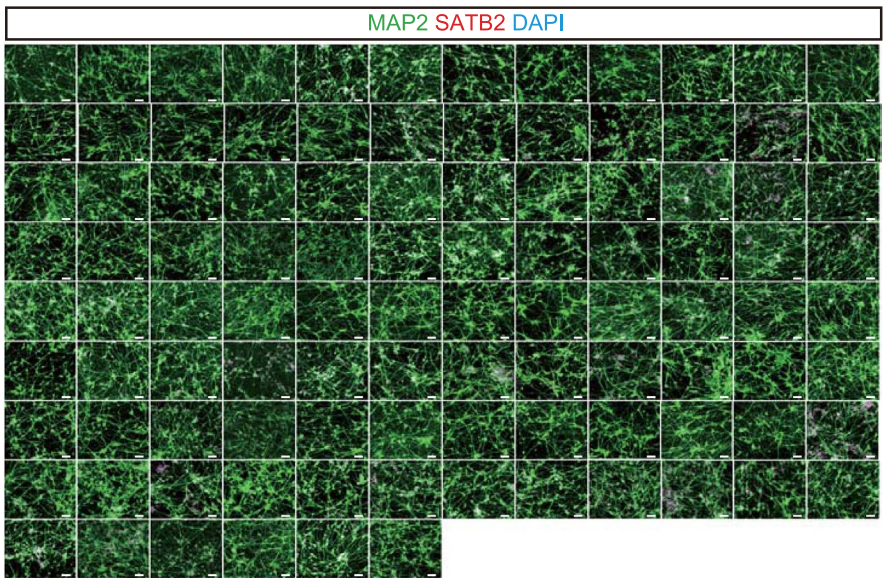

e

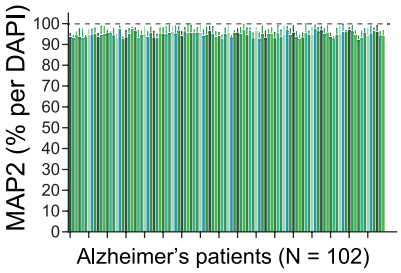

f

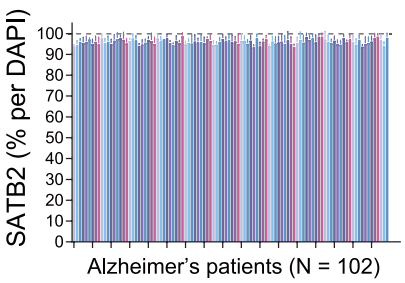

Extended Data Fig. 1 | See next page for caption.

Extended Data Fig. 1 | Establishment of cortical neurons from iPSCs of patients with sporadic AD. (a) Clinical information of patients who provided somatic cells as resource for iPSC establishment. (b) Generated iPSC lines expressed pluripotency markers TRA1-60 (green) and NANOG (red). Representative images from three independent experiments were shown. Nuclei were stained with 4′,6-diamidino-2-phenylindole: DAPI (blue). Scale bars = 200 μm. (c) Schema of differentiation method and assay (d) iPSC-derived neurons expressed excitatory cortical neuron markers, including MAP2 (green) and TBR2 (red) on day 8 of differentiation. Representative images from three independent experiments were shown. Scale bars = 50 μm. Purity of day 8 cortical neurons was shown as positivity for MAP2 (e) and SATB2 (f) with no significant variation among different patients ($p = 0.7727$ for MAP2, $p = 0.3675$ for SATB2, one way ANOVA). Data represent mean ± SD ($n = 3$ for each patient clone).

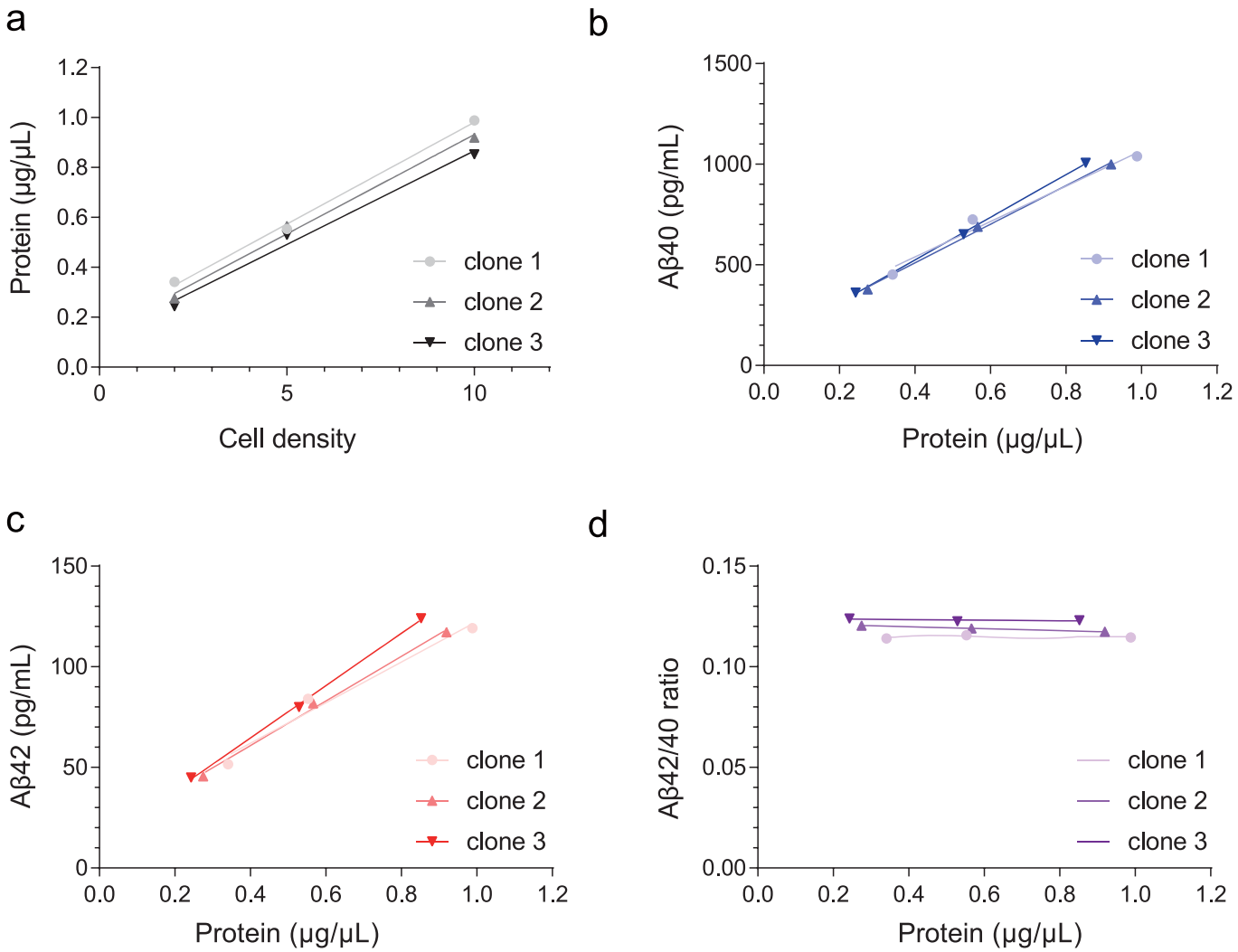

Extended data Fig. 2 | Correlation between total protein concentration and cell density or Aβ species. (a) Correlation plot between total protein concentration (µg/µL), Y-axis and disseminated cell density (10^4 cells per well of 96-well-plate). Linear fit (grey lines) is shown for three different clones from three different patients (n = 3 per clone). (b) Correlation plot between Aβ40 (pg/mL), Y-axis and total protein concentration (µg/µL), X-axis. Linear fit (blue lines) is shown for three different clones from three different patients (n = 3 per clone). (c) Correlation plot between Aβ42 (pg/mL), Y-axis and total protein concentration (µg/µL), X-axis. Linear fit (blue lines) is shown for three different clones from three different patients (n = 3 per clone). (d) Correlation plot between Aβ42/40 ratio, Y-axis and total protein concentration (µg/µL), X-axis. Linear fit (blue lines) is shown for three different clones from three different patients (n = 3 per clone).

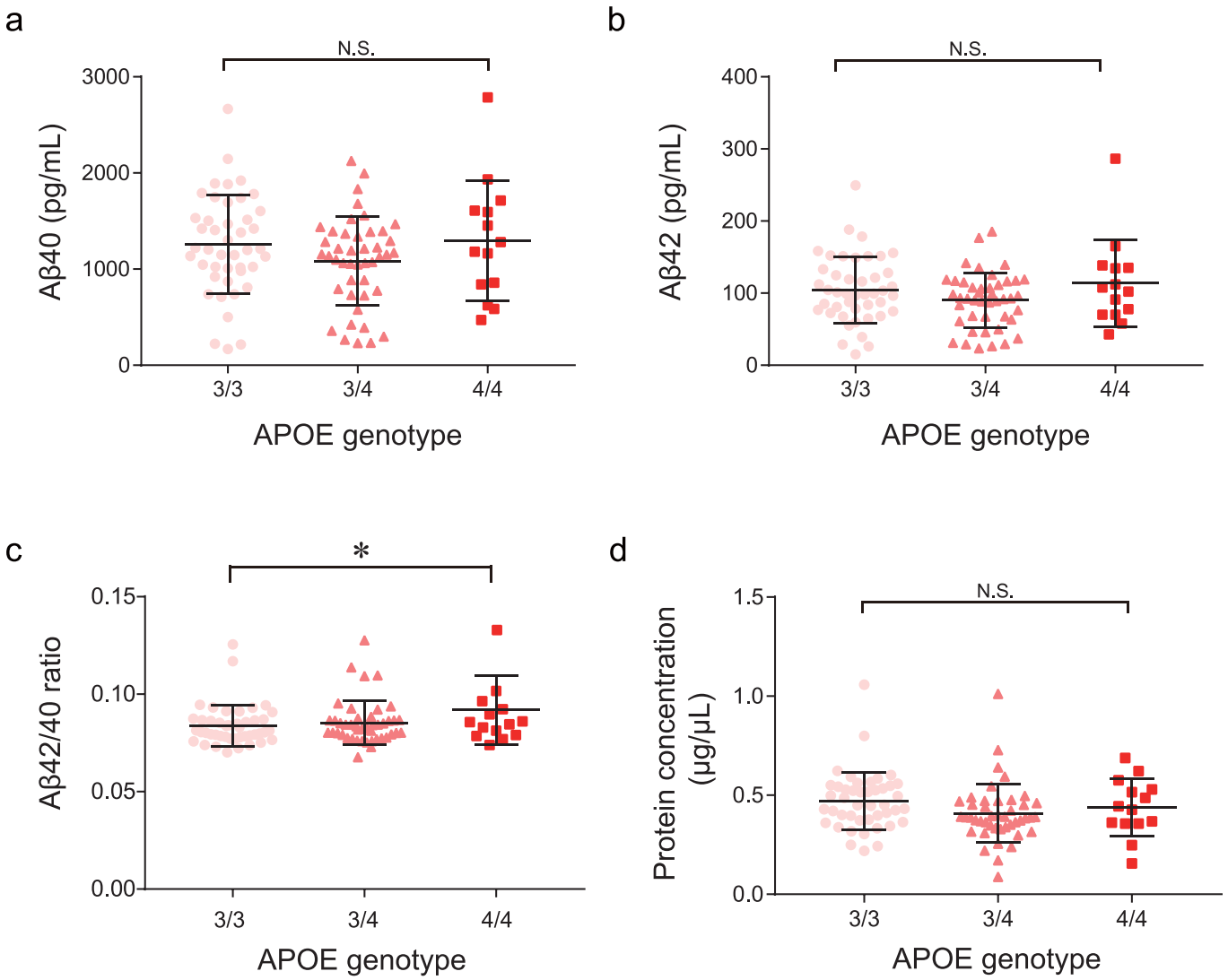

Extended Data Fig. 3 | Comparison of *APOE* genotype and Aβ phenotypes in induced cortical neurons from AD iPSCs. Plots show the distribution of (a) Aβ40, (b) Aβ42, (c) Aβ42/40 ratio and (d) protein concentration among different genotypes. X-axes correspond to *APOE* ε4 genotypes (patients, N = 44 for APOE3/3, N = 44 for APOE3/4, N = 14 for APOE4/4) and Y-axes represent (a) Aβ40 amounts, (b) Aβ42 amounts, (c) Aβ42/40 ratio, and (d) protein concentration of iPSC-derived cortical neurons. Horizontal lines are the median weights within a genotypic group, and error bars indicate standard deviation (S.D.). $p > 0.05$: not significant (N.S.) (one-way ANOVA with (two-way ANOVA with Tukey's multiple comparisons test). Abbreviation: *APOE*, Apolipoprotein E.

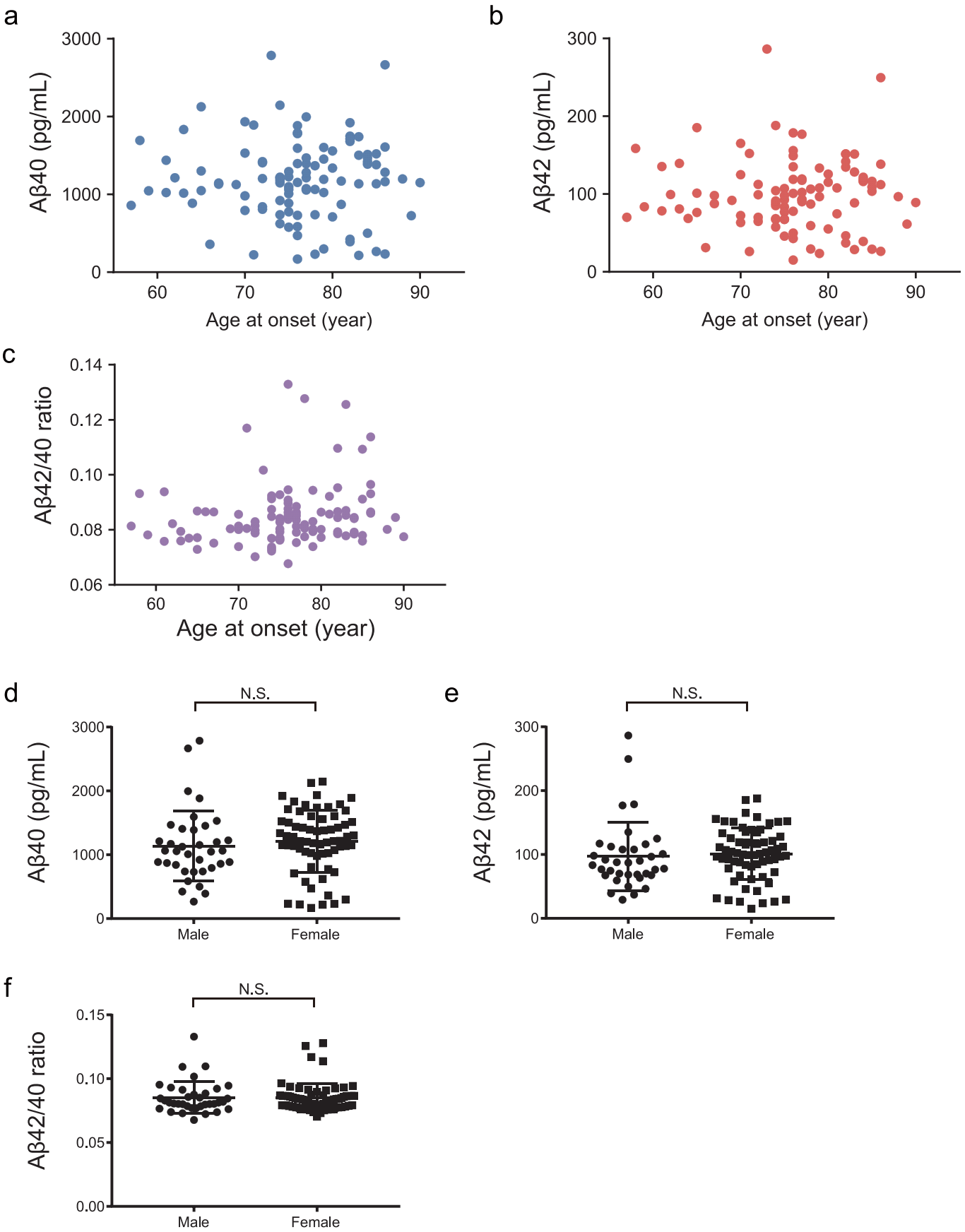

Extended Data Fig. 4 | See next page for caption.

Extended Data Fig. 4 | There was no significant correlation between Aβ phenotypes in AD iPSC-derived cortical neurons and clinical status. Scatter plots (N = 102) show Aβ phenotypes, including (a) Aβ40 (left panel, blue), (b) Aβ42 (right panel, red), and (c) Aβ42/40 ratio (Y-axis). X-axis shows the onset age of cognitive dysfunction. The scatter plot does not show statistically significant correlation between Aβ phenotypes and age at onset (R-squared = 0.03, p-value = 0.074 for Aβ40; R-squared = 0.000030, p-value = 0.87 for Aβ42; R-squared = 0.000023, p-value = 0.96 for Aβ42/40 ratio). The plots show the distribution of Aβ phenotypes between genders. X-axes correspond to gender, male or female (patients, n = 36 for male, n = 66 for female), and y-axes represent (d) Aβ40 dose, (e) Aβ42 dose, and (f) Aβ42/40 ratio in the culture supernatant of iPSC-derived cortical neurons. Horizontal lines are the median weights within a genotypic group, and error bars indicate standard deviation (S.D.).

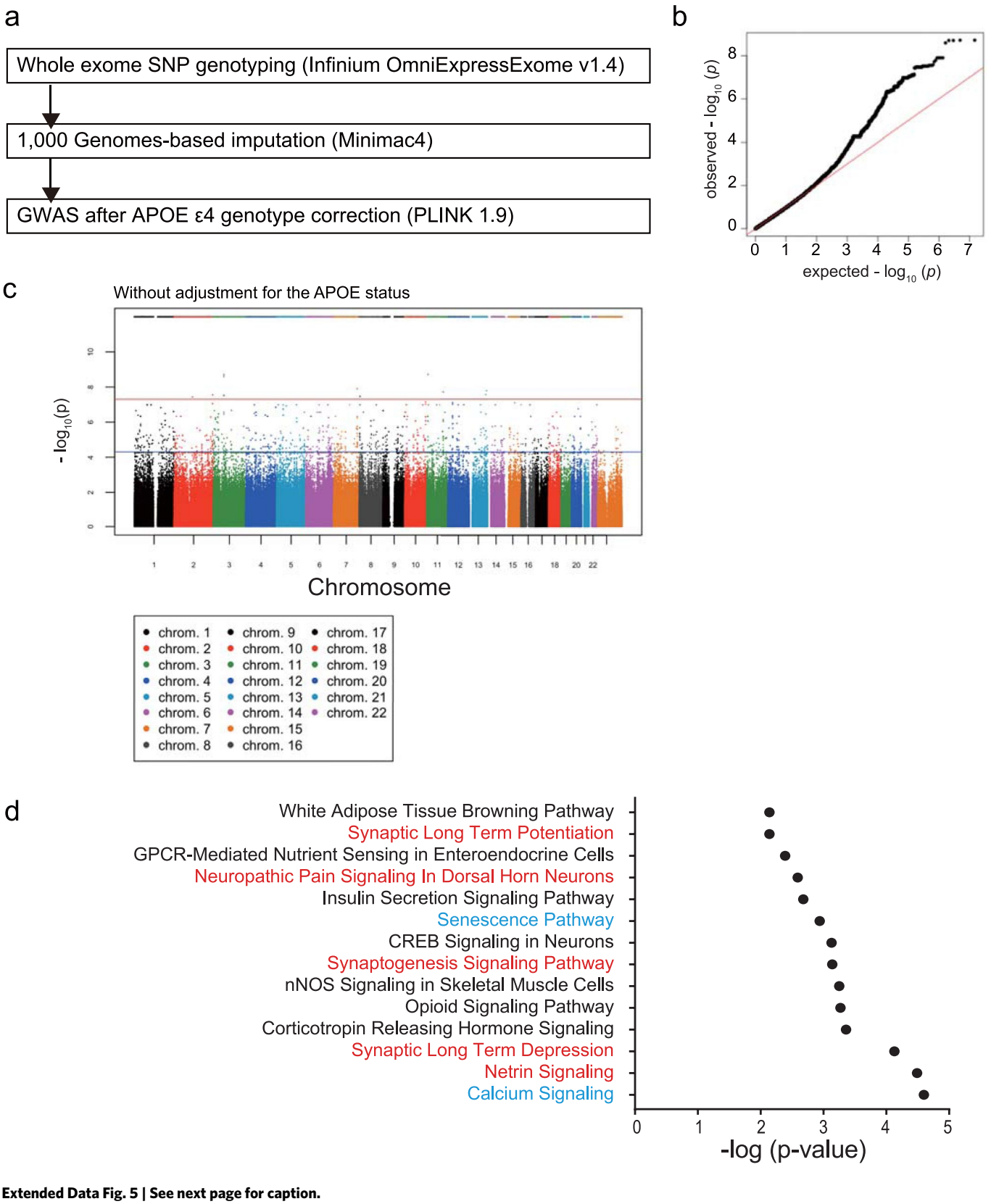

Extended Data Fig. 5 | See next page for caption.

Extended Data Fig. 5 | Cellular dissection of polygenicity identified the genetic loci and molecular pathway related with Aβ42/40 ratio in AD cortical neurons. (a) Flowchart for genome-wide analysis. (b) Quantile-quantile (Q-Q) plot of observed – $\log_{10}$ (p-value) from genome-wide association analysis of Aβ42/40 ratio level versus those expected under null hypothesis. Genomic inflation factor (λ) was 0.9659, suggesting that there was no population stratification effect. (c) Genome-wide association study for CDiP was conducted to identify the genetic loci related to the Aβ42/40 ratio without adjustment for the *APOE* status. Linear association between SNPs and the Aβ42/40 ratio was analyzed. Manhattan plot showing observed –$\log_{10}$ (p-value) of all tested SNPs with Aβ42/40 ratio (y-axis). Chromosomes are shown on the x-axis. The red line corresponds to genome-wide Bonferroni-corrected significance threshold $p < 5 \times 10^{-8}$. (d) Pathway analysis for 24 genes, identified in CDiP with Aβ42/40 ratio A selection of top canonical pathways found using Ingenuity Pathway Analysis (IPA) package to identify the enriched canonical pathways which were significantly enriched by using gene sets, identified in CDiP with Aβ42/40 ratio. Pathway analysis identified 14 pathways ($p < 0.01$), including 5 neuron-related pathways (red) and 2 pathways known to alter Aβ production (blue). Horizontal axis = p-value by Fisher's exact test of pathway analysis.

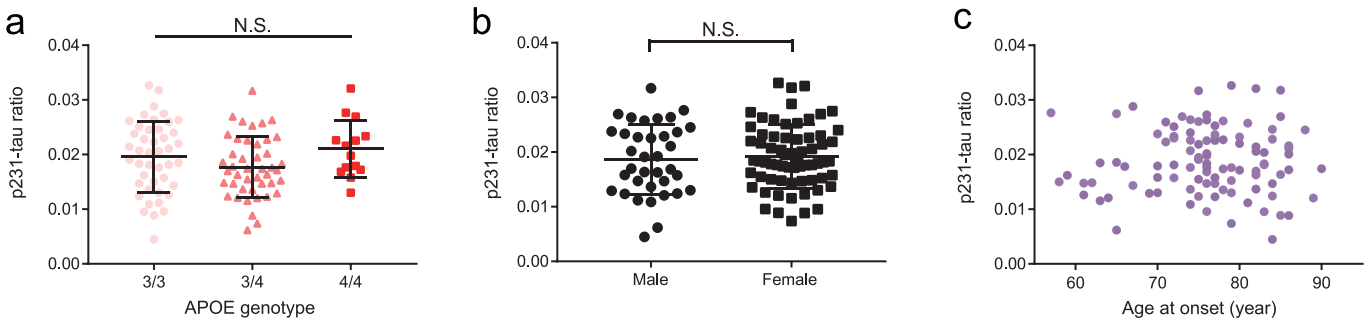

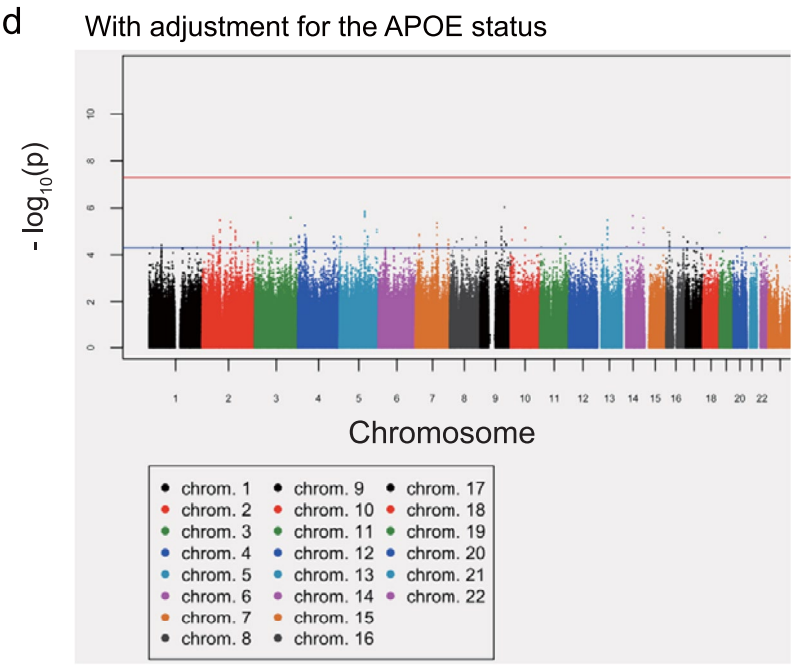

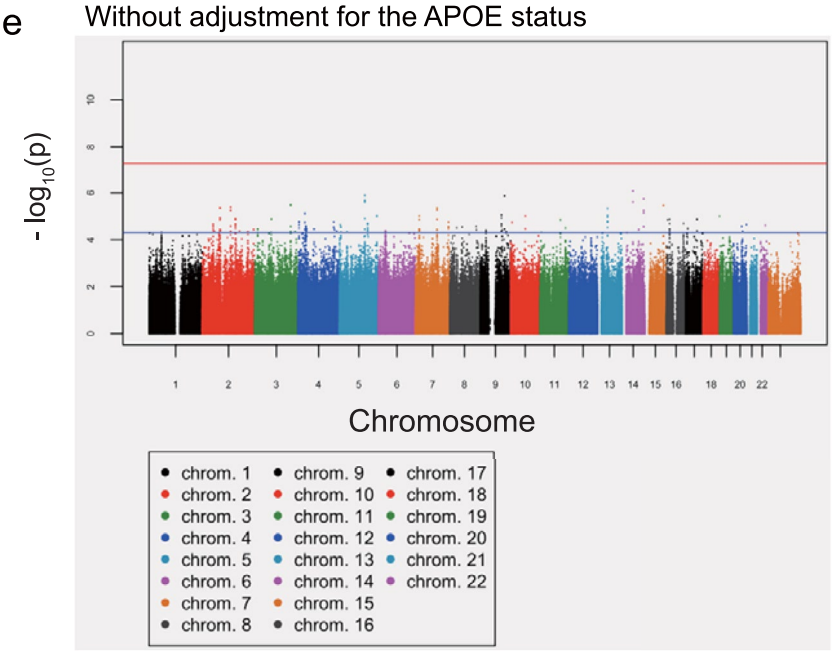

Extended Data Fig. 6 | See next page for caption.

Extended Data Fig. 6 | CDiP for p231-phosphorylated tau / total tau ratio of AD cortical neurons. (a) Plots show the distribution of the p231-tau / total tau ratio (p231-tau ratio) among different *APOE* genotypes. X-axes correspond to *APOE* ε4 genotypes (patients, n = 44 for APOE3/3, n = 44 for APOE3/4, n = 14 for APOE4/4), and Y-axes represent p231-tau ratio of iPSC-derived cortical neurons. Horizontal lines are the median weights within a genotypic group, and error bars indicate S.D. (b) The plots show the distribution of p231-tau ratio between genders. X-axes correspond to gender, male or female (patients, n = 36 for male, n = 66 for female), and y-axes represent p231-tau ratio of iPSC-derived cortical neurons. Horizontal lines are the median weights within a genotypic group, and error bars indicate S.D. (c) Scatter plots (N = 102) of p231-tau ratio (Y-axis) and onset ages of cognitive dysfunction (X-axis). The scatter plot does not show statistically significant correlation between p231-tau ratio and age at onset. (d) Genome-wide association study for CDiP was conducted to identify the genetic loci related to the p231-tau ratio with adjustment for the *APOE* status. Linear association between SNPs and the p231-tau ratio was analyzed. Manhattan plot showing observed $-\log_{10}$ (p-value) of all tested SNPs with p231-tau ratio (Y-axis). The red line corresponds to genome-wide Bonferroni-corrected significant threshold $p < 5 \times 10^{-8}$. (e) Genome-wide association study for CDiP was conducted to identify the genetic loci related to the p231-tau ratio without adjustment for the *APOE* status. Linear association between SNPs and the p231-tau ratio was analyzed. Manhattan plot showing observed $-\log_{10}$ (p-value) of all tested SNPs with p231-tau ratio (Y-axis). The red line corresponds to genome-wide Bonferroni-corrected significant threshold $p < 5 \times 10^{-8}$.

a

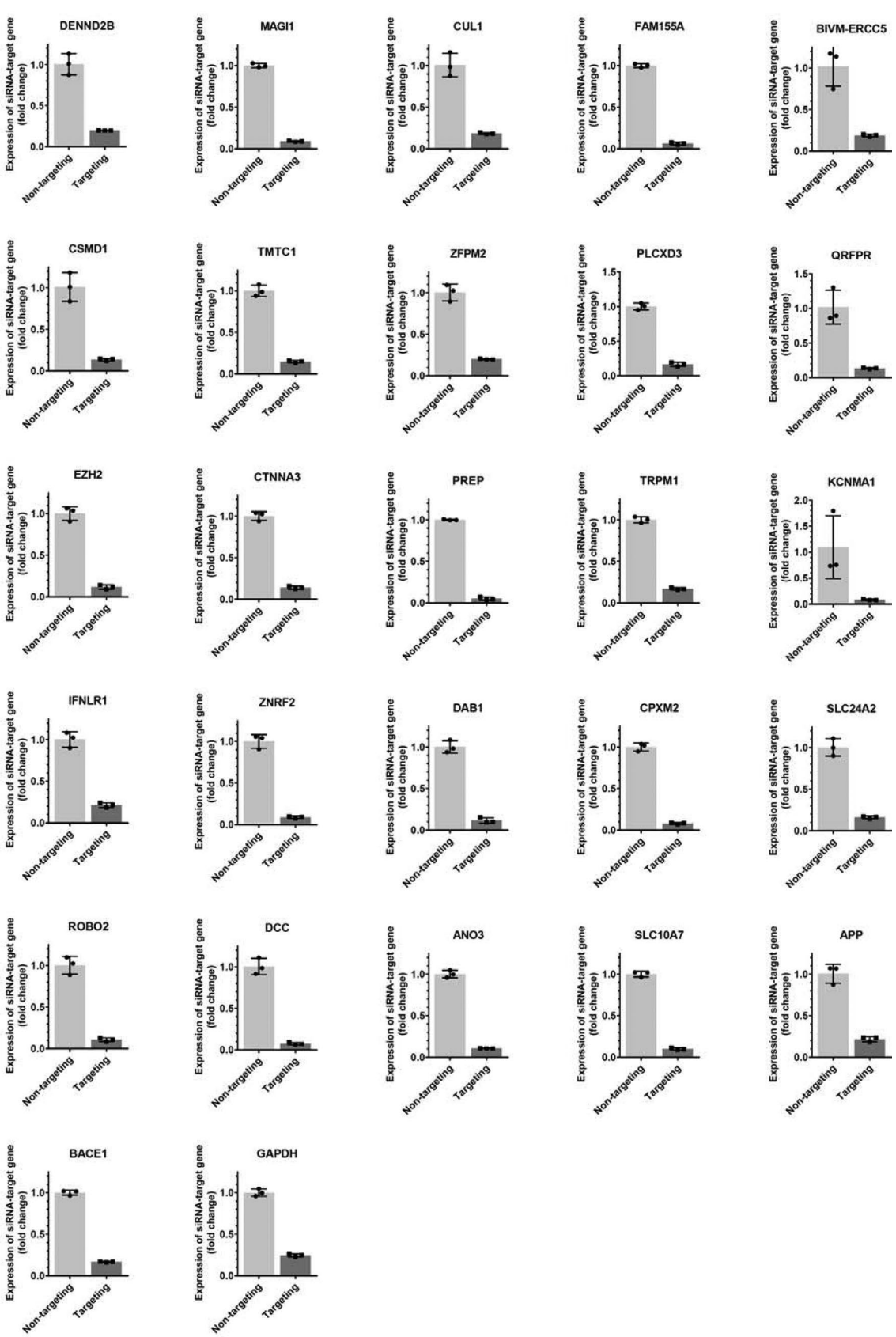

Extended Data Fig. 7 | Alteration of gene expression by siRNA treatment. (a) Relative expression of target gene for siRNA treatment was quantified. Y-axis shows fold change VS. non-targeted control siRNA. Data represent mean ± S.D. (n = 2 for each target gene).

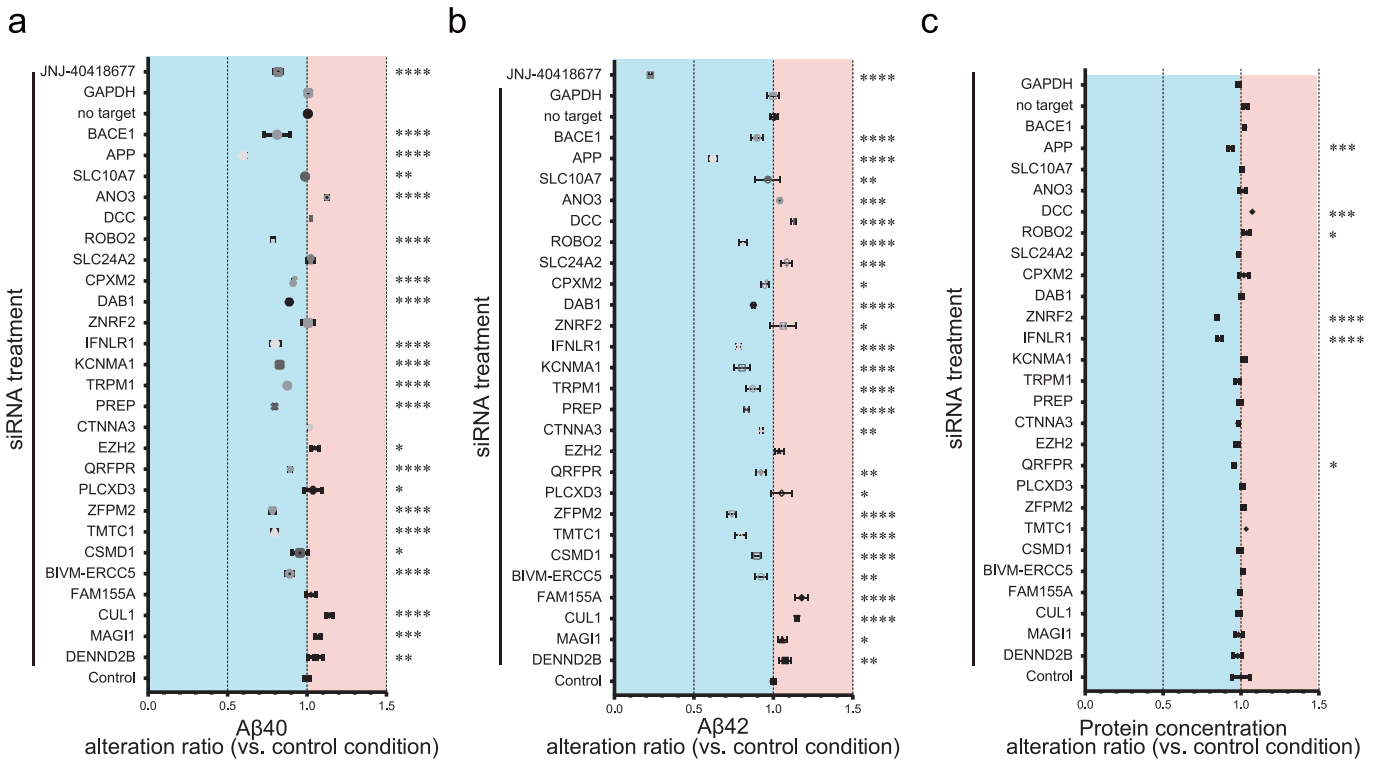

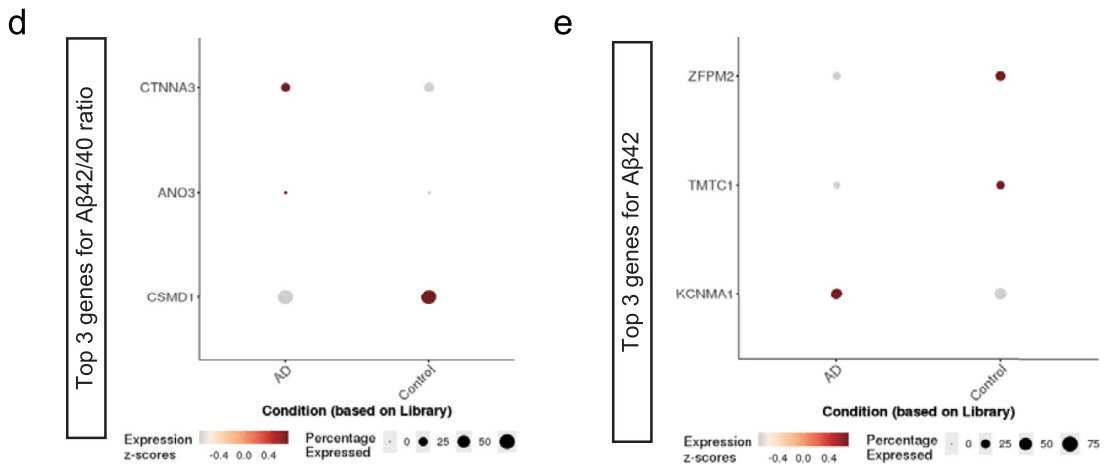

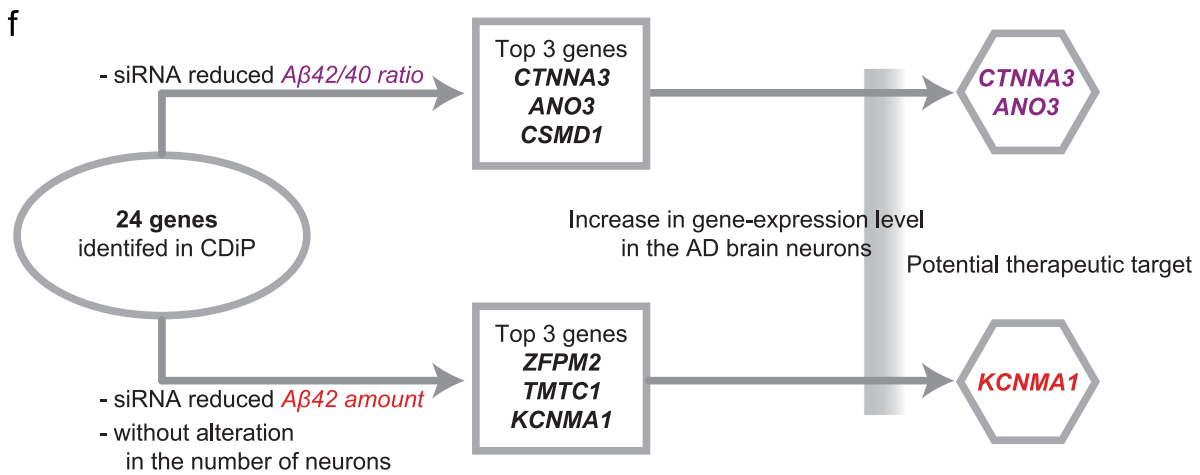

Extended Data Fig. 8 | See next page for caption.

Extended Data Fig. 8 | Genes identified by CDiP can be potential therapeutic targets for Aβ phenotypes. (a) Aβ40, (b) Aβ42, and (c) total protein concentration was analyzed after siRNA treatment, which targeted identified genes in cellular dissection of polygenicity (CDiP), Aβ-related genes, including APP, and BACE1. Non-target siRNA was used as negative control. JNJ-40418677 1 μM, second generation of γ-secretase modulator (GSM) to suppress Aβ production, was used as positive control for altered Aβ phenotypes. X-axis shows alteration level in Aβ40 compared with non-treatment control (n = 2 biological replicates). Shown is mean ± S.D. $p < 0.05$: *; $p < 0.01$: **; $p < 0.001$: ***.; $p < 0.0001$: **** (one way ANOVA with Uncorrected Fisher's LSD) (d) Comparing neuronal expression of genes, whose siRNA altered the Aβ42/40 ratio, between the brains of Alzheimer's disease and non-demented control. Transcriptome data from *Single-cell atlas of the Entorhinal Cortex in Human Alzheimer's Disease* was analyzed. (e) Comparison of neuronal expression of genes whose siRNA reduced Aβ42, between the brains of Alzheimer's disease and non-demented control. (f) The single-cell-based transcriptome data of six AD brains and six control brains, which provide the transcriptome data for individual cell types, was utilized to investigate the expression status of focused genes. Genes with higher expression in AD brains were selected as the potential therapeutic target.

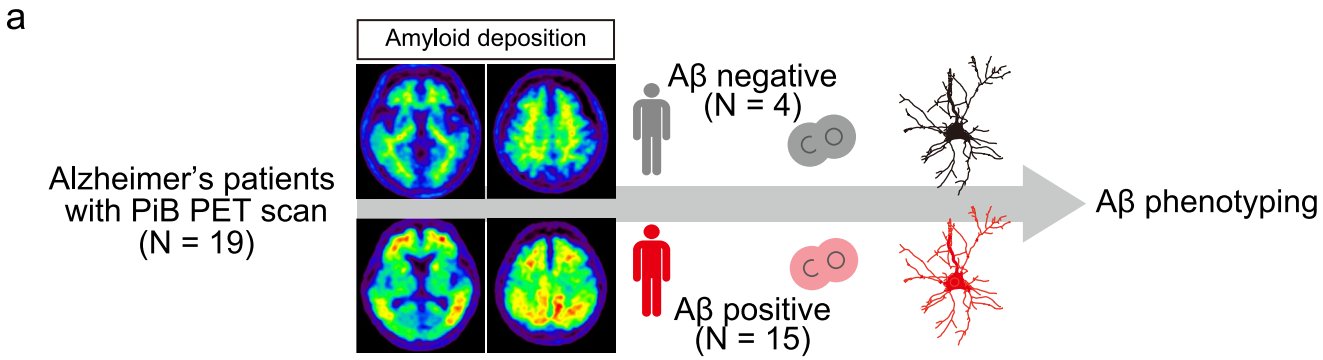

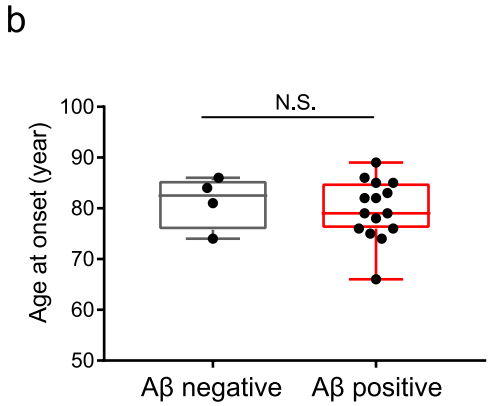

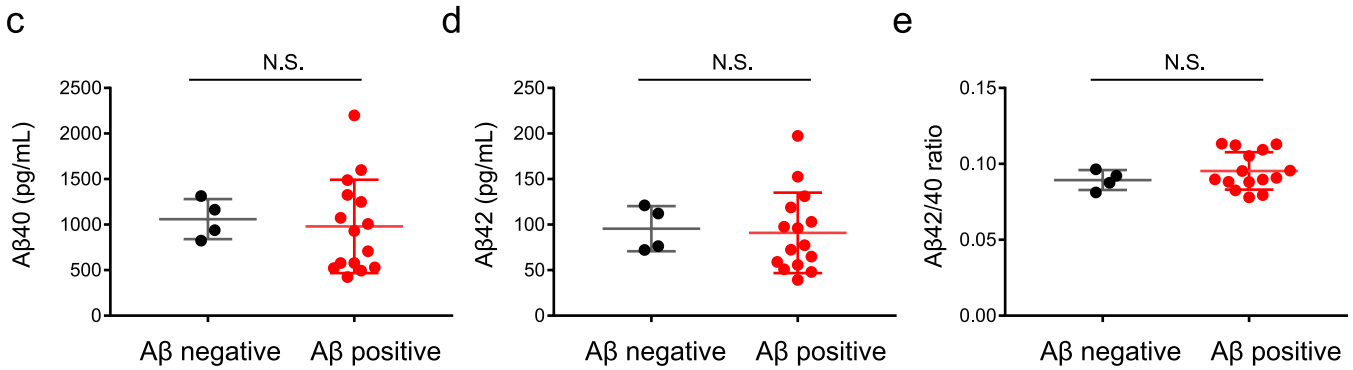

f

J-ADNI data (N = 407)

status	number of participants
Control	152
AD	255

ADNI data (N = 479)

status	number of participants
Control	233
AD	246

KCNMA1
with rare variants in AD

Extended Data Fig. 9 | See next page for caption.

Extended Data Fig. 9 | Clinical status of Aβ deposition in brain did not correlate with Aβ phenotypes in induced cortical neurons from AD iPSCs. (a) Schema of small cohort (N = 19), including the clinical status of Aβ deposition, measured by PiB-PET. (b) There was no difference in age at onset between Aβ-negative and Aβ-positive patients. The box and whiskers plot showed the range (whiskers) from minimum to maximum, the median (horizontal line) and the 25% and 75% (box) percentiles. Clinical status of Aβ deposition in the brain did not affect Aβ phenotypes in induced cortical neurons, from human iPSCs including (c) Aβ40, (d) Aβ42, and (e) Aβ42/40 ratio (patients, n = 4 for Aβ negative, n = 15 for Aβ positive). Horizontal lines are the median weights within groups, and error bars indicate standard deviation (S.D.). (f) J-ANDI and ADNI population for investigating rare variants of Alzheimer's disease. Abbreviation: PiB PET: Pittsburgh Compound-B positron emission tomography, ANDI: Alzheimer's Disease Neuroimaging Initiative, J-ANDI: Japanese ADNI.

a

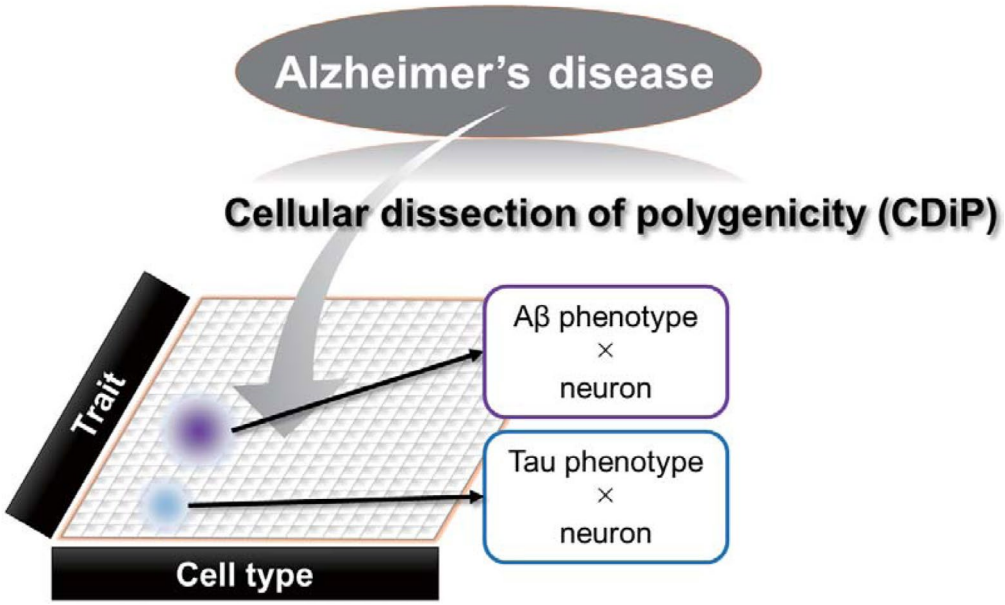

Extended Data Fig. 10 | Dissecting Alzheimer's pathology into cellular polygenic architecture of the pathological traits to reveal the polygenicity of AD. (a) CDiP can provide the information of genetic background, linked to each cell-type and trait in Alzheimer's pathology.

nature portfolio

Corresponding author(s): Haruhisa Inoue

Last updated by author(s): Oct 22, 2021

Reporting Summary

Nature Portfolio wishes to improve the reproducibility of the work that we publish. This form provides structure for consistency and transparency in reporting. For further information on Nature Portfolio policies, see our Editorial Policies and the Editorial Policy Checklist.

Statistics

For all statistical analyses, confirm that the following items are present in the figure legend, table legend, main text, or Methods section.

n/a	Confirmed
☐	☒ The exact sample size (*n*) for each experimental group/condition, given as a discrete number and unit of measurement
☐	☒ A statement on whether measurements were taken from distinct samples or whether the same sample was measured repeatedly
☐	☒ The statistical test(s) used AND whether they are one- or two-sided *Only common tests should be described solely by name; describe more complex techniques in the Methods section.*
☒	☐ A description of all covariates tested
☐	☒ A description of any assumptions or corrections, such as tests of normality and adjustment for multiple comparisons
☐	☒ A full description of the statistical parameters including central tendency (e.g. means) or other basic estimates (e.g. regression coefficient) AND variation (e.g. standard deviation) or associated estimates of uncertainty (e.g. confidence intervals)
☐	☒ For null hypothesis testing, the test statistic (e.g. *F*, *t*, *r*) with confidence intervals, effect sizes, degrees of freedom and *P* value noted *Give P values as exact values whenever suitable.*
☒	☐ For Bayesian analysis, information on the choice of priors and Markov chain Monte Carlo settings
☒	☐ For hierarchical and complex designs, identification of the appropriate level for tests and full reporting of outcomes
☒	☐ Estimates of effect sizes (e.g. Cohen's *d*, Pearson's *r*), indicating how they were calculated

Our web collection on statistics for biologists contains articles on many of the points above.

Software and code

Policy information about availability of computer code

Data collection	IN cell analyzer 6000 (GE Healthcare) Sector Imager 2400 (Meso Scale Discovery)
Data analysis	GenomeStudio (Illumina) Ingenuity Pathway Analysis (IPA, version IPA Spring Release (March 2021), QIAGEN) BWA-MEM version 0.7.15-r1140 snpEff version 4.3t R package seqMeta version 1.6.7 GraphPad Prism (version 7.0, GraphPad, San Diego, CA)

For manuscripts utilizing custom algorithms or software that are central to the research but not yet described in published literature, software must be made available to editors and reviewers. We strongly encourage code deposition in a community repository (e.g. GitHub). See the Nature Portfolio guidelines for submitting code & software for further information.

Data

Policy information about availability of data

All manuscripts must include a data availability statement. This statement should provide the following information, where applicable:

- Accession codes, unique identifiers, or web links for publicly available datasets
- A description of any restrictions on data availability
- For clinical datasets or third party data, please ensure that the statement adheres to our policy

Data used in the preparation of this article were obtained from the Alzheimer's Disease Neuroimaging Initiative (ADNI) database (adni.loni.usc.edu). ADNI was launched in 2003 as a public-private partnership, led by Principal Investigator Michael W. Weiner, MD. The primary goal of ADNI has been to test whether serial magnetic resonance imaging (MRI), positron emission tomography (PET), other biological markers, and clinical and neuropsychological assessments can be combined to measure the progression of mild cognitive impairment (MCI) and early Alzheimer's disease (AD). SNP array data is available in The National Bioscience Database Center (NBDC) (https://humandbs.biosciencedbc.jp/en/, research ID: hum0314.v1). All data generated or analysed during this study are included in this published article (and its supplementary information files).

Field-specific reporting

Please select the one below that is the best fit for your research. If you are not sure, read the appropriate sections before making your selection.

☒ Life sciences ☐ Behavioural & social sciences ☐ Ecological, evolutionary & environmental sciences

For a reference copy of the document with all sections, see nature.com/documents/nr-reporting-summary-flat.pdf

Life sciences study design

All studies must disclose on these points even when the disclosure is negative.

Sample size	For establishment of induced pluripotent stem cells (iPSC) and genome-wide association studies, the number of iPSC clones were determined empirically to satisfy the statistically appropriate analysis. No statistical methods were used to pre-determine sample sizes but our sample sizes are similar to those reported in previous publications (J. Adv. Res. 22, 119–135 (2019).).
Data exclusions	No data was excluded.
Replication	We replicated analysis using 2-3 independent experiments. For the investigation of rare variants, we analyzed two cohorts, J-ADNI and US-ADNI.
Randomization	No allocation into different condition group were performed, therefore randomization is not relevant to this study.
Blinding	Group assignments were not blinded because we did not use the data from clinical prospective studies.

Reporting for specific materials, systems and methods

We require information from authors about some types of materials, experimental systems and methods used in many studies. Here, indicate whether each material, system or method listed is relevant to your study. If you are not sure if a list item applies to your research, read the appropriate section before selecting a response.

Materials & experimental systems

n/a	Involved in the study
☐	☒ Antibodies
☐	☒ Eukaryotic cell lines
☒	☐ Palaeontology and archaeology
☒	☐ Animals and other organisms
☐	☒ Human research participants
☐	☒ Clinical data
☒	☐ Dual use research of concern

Methods

n/a	Involved in the study
☒	☐ ChIP-seq
☒	☐ Flow cytometry
☒	☐ MRI-based neuroimaging

Antibodies

Antibodies used	Immunocytochemistry, NANOG (1:100 dilution; Abcam ab80892, Cambridge, UK), TRA1-60 (1:400; CST #4746, Danvers, MA), MAP2 (1:4,000; Abcam ab5392), SATB2 (1:400; Abcam EPNCIR130A ab92446), Alexa 488-conjucated antibody (1:400, Thermofisher A11029), Alexa 488-conjucated antibody (1:400, Thermofisher A11039), Alexa 594-conjucated antibody (1:400, Thermofisher A21207)

Validation	All antibodies were previously validated for same application (Cell Rep . 2017 Nov 21;21(8):2304-2312.).

Eukaryotic cell lines

Policy information about cell lines

Cell line source(s)	Induced pluripotent stem cells established from patients with sporadic Alzheimer's disease
Authentication	None of the cell lines used were authenticated.
Mycoplasma contamination	All cell lines tested negative for mycoplasma contamination
Commonly misidentified lines (See ICLAC register)	not available

Human research participants

Policy information about studies involving human research participants

Population characteristics	In this study, samples from 102 patients with sporadic Alzheimer's disease were utilized. Detailed information is given in Tables and methods section.
Recruitment	This study itself dose not directly involve participant recruitment.
Ethics oversight	For the establishment of iPSCs from human peripheral blood mononuclear cells (PBMCs), PBMCs of patients with Alzheimer's disease were collected according to the research project, which was approved by the Ethics Committee of the Department of Medicine and Graduate School of Medicine, Kyoto University (approval no. = R0091, G259, and G0722). Written, informed consent is obtained from all participants in this study.

Note that full information on the approval of the study protocol must also be provided in the manuscript.

Clinical data

Policy information about clinical studies

All manuscripts should comply with the ICMJE guidelines for publication of clinical research and a completed CONSORT checklist must be included with all submissions.

Clinical trial registration	We used a subset of the ADNI dataset (NCT00106899).
Study protocol	Available on the web site of ADNI (http://adni.loni.usc.edu/).
Data collection	ADNI data are collected as described on the web site (http://adni.loni.usc.edu/).
Outcomes	The outcome in this study was prediction of clinical data in ADNI datasets.